IDRiM (2026) 16 (1) **ISSN: 2185-8322**
DOI10.5595/001c158819

Journal of Integrated Disaster Risk Management

Regular Article

Integrated Remote Sensing Approach for Multi-Hazard Zonation in Rishiganga-Dhauliganga Valley, Uttarakhand, India

Rabisankar Karmakar[1*], Uday Kumar Ghosh[2], Pawan Kumar[3], Mrinmoy Kumar Das[1], Joyasree Sinha Chakrabarti[2], Animesh Thakur[4], K. Aravind[2], Akshaya Kumar Mishra[5], and Saibal Ghosh[6]

Received: 14/02/2025 / Accepted: 15/10/2025 / Published online: 27/03/2026

Abstract Multi-hazard studies in the Himalayas are crucial due to the region's vulnerability to a range of natural hazards that often interact in complex and dynamic ways. These studies emphasize the need for integrated risk management, early warning systems, and adaptation strategies to cope with the combined impacts of these hazards. With the increasing impacts of climate change and rapid urbanization, these risks are expected to intensify, making ongoing research and proactive planning essential for ensuring the resilience of Himalayan communities. The present study focuses on a region located in the higher Himalayas, characterized by a complex morphometric setup and landforms, produced by the interplay of both glacial and fluvial geomorphic processes within an active Fold-Thrust-Belt. In this study, multisensor and temporal earth observation data, along with advanced remote sensing and GIS techniques, were used for a macro-scale multi-hazards zonation study encompassing snow avalanche, landslide, and earthquake disasters. The snow avalanche susceptibility map is derived through the Analytical Hierarchy Process (AHP), while the landslide susceptibility has been prepared using the Weighted Multiclass Index Overlay method. The seismic hazard map has also been derived through AHP. The resulting integrated multi-hazard map, which overlays the individual hazard levels, indicates that 16% of the study area falls within a low hazard zone. Hazard-specific zones cover 17% for earthquakes, 17% for avalanches, and 24% for landslides. Notably, approximately 46% of the study area is exposed to multiple hazard types. The findings of this study, combined with multi-hazard susceptibility modelling in such remote and challenging terrain, will serve as crucial inputs for stakeholders to develop effective mitigation

[1] Landslide Studies Division, Central Headquarters, Geological Survey of India
[2] Photogeology and Remote Sensing, Central Headquarters, Geological Survey of India
[3] Glaciology, Northern Region, Geological Survey of India
[4] Geodynamic Studies Division, Central Headquarters, Geological Survey of India
[5] Geohazards Research and Management Cell, Central Headquarters, Geological Survey of India
[6] M IV-Multi-disciplinary Geosciences, Geological Survey of India
* Corresponding author email: rabi.geoju@gmail.com

strategies, implement early warning systems, and guide land use planning in response to multi-hazard scenarios.

Keywords: multi-hazard, susceptibility, AHP, DSHA, Weighted Multiclass Index Overlay

1. INTRODUCTION

The Himalayan region, known for its complex geological and ecological dynamics, is highly vulnerable to a range of natural hazards (Gautam, et al., 2013; Kala, 2014; Pathak et al., 2019) that often occur simultaneously or in quick succession, complicating risk management efforts. These hazards include earthquakes, landslides, floods, glacial lake outburst floods (GLOFs), avalanches, and extreme weather events. Each year, these multiple hazards result in fatalities and infrastructural damage (Chouhan et al., 2022a). A single natural disaster can trigger or increase the likelihood of additional hazards (Jinxing et al., 2002; Bathrellos et al., 2017).

The assessment of a single hazard will not serve the problem in addressing the risk mitigation strategies where the area is affected by multiple hazards (Sekhri et al, 2020). Multi-hazard risk assessment, which evaluates the combined likelihood of experiencing extreme natural events across multiple hazards, can be valuable for managing the interactions between these hazards (Kappes et al., 2012; Gill & Malamud, 2016). There is plethora of works on individual natural hazards assessment such as landslides (Guzzetti et al.,1999; Van Westen et al., 2006; Ghosh, 2011; Bhandari & Wankhade, 2025), earthquakes (Khattri et al., 1984; Bhatia et al., 1999; Mahajan et al., 2010; Kumar et al., 2011; Nath & Thingbaijam, 2012; Rout et al., 2018; Sharma & Sarkar, 2023), avalanche (Snehmani et al., 2013; Kumar et al., 2019; Xi & Mei, 2023). Since the United Nations emphasized the importance of multi-hazard studies for risk assessment in 2002 and its subsequent addressing in Hyogo framework for action (UN-ISDR, 2005), SENDAI framework of Disaster Risk Reduction in 2015–2030 (UNISDR, 2015) there has been a notable increase in research focused on multi-hazard approaches. With advent of GIS and RS technology, researchers adopted various methodologies in developing multi-hazard susceptibility using two and more natural hazards like Bathrellos et al. (2017) carried out the multi-hazard assessment in Greece considering the landslide, flood, and seismic hazards using Analytical Hierarchy Process (AHP). In a similar line Skilodimou et al. (2019) in Greece; Aksha et al. (2020) in Nepal assess the landslides, earthquakes, and floods. Pourghasemi et al. (2019) conducted study in Iran using the SWARA-ANFIS-GWO model to address the landslide, earthquake, and flood hazards. Yousefi et al. (2020) applied machine learning algorithm to assess the snow avalanches, landslides, wildfires, land subsidence, and floods in Iran. Rehman et al. (2022) evaluate the landslides and flood hazards in Muzaffarabad, Pakistan using the AHP and Frequency Ratio (FR) whereas Akbar et al. (2023) utilized FR to analysis the flood, landslide, and snow avalanches in Kargil-Ladakh. Rusk et al. (2022) studied floods, landslides, and wildfires in Hindukush Himalaya through maximum entropy method. Ullah et al. (2022) evaluate landslides, flash floods, and debris flows in the Shangla District, Pakistan, with CNN, LR, and KNN. Sharma and Rana (2024) applied AHP for multi-hazard study in

Jammu encompassing landslides, floods, earthquakes, droughts, forest fires and soil erosion. In another work Sharma et al. (2024) conducted multi-hazard susceptibility analysis in Jammu division using the FR and Shannon entropy considering the earthquake, foods, landslide, drought and forest fire. Gupta et al. (2024) applied the Random Forest and Artificial Neural Network approach to study landslide and earthquake susceptibility respectively. Finally, combined both the maps using the matrix approach. Despite several works in the Himalaya on multi-hazard assessment, the study of interplay and cascading effects of avalanche, earthquake, and landslide has not been dealt earlier. Ali et al. (2022) prepared a disaster catalogue for Kashmir valley encompassing earthquakes, flood, landslide, and snow avalanche. To fill this research gap there is a need for a region specific straightforward, easy to employ multi-hazard zonation methodology covering snow avalanche, landslide, and earthquake in data scarce, remotely located areas for future planning.

In the past decades, the Indian Himalayan Region has experienced number of multiple hazards generated due to the domino and cascading effects of a single natural hazard. The notable such incidences are the 18 September 2011 Sikkim earthquake resulting landslide induced losses in terms of life, property, and infrastructure (Baruah et al., 2018), 16-17 June 2013 Kedarnath disaster due to heavy rainfall resulting landslides and floods in the downstream claiming more than 5000 life, damages to infrastructure (Kumar et al., 2016), the devastating flash flood of Rishiganga-Dhauliganga valley in Chamoli district, Uttarakhand, on February 7, 2021 resulted in a catastrophic deluge downstream, resulting in a large death toll and wrecking of two ongoing hydroelectric power projects in Raini and Tapovan villages (Shugar et al., 2021). These incidents and the increasing trend of their occurrences in the recent past (Rehman et al., 2022) have raised urgent concerns about the need for multi-hazard study considering the frequent occurrences of avalanche, earthquake, and landslide in this terrain towards effective action planning to ensure safe and sustainable development in the Himalayan mountainous region.

The present study aimed to integrate the individual natural hazards, such as landslides, snow avalanches, and earthquakes to create a comprehensive multi-hazard map for Rishiganga and Dhauliganga valleys of Chamoli district, Uttarakhand. The work utilized multi-sensor and temporal Earth observation data, combined with advanced remote sensing and GIS techniques, to conduct a macro-scale multi-hazard zonation analysis. The study first evaluated the susceptibility to individual natural hazards and, subsequently, all the hazards were integrated to create a comprehensive multi-hazard map using the Analytical Hierarchy Process (AHP) developed by Saaty (1980, 2000).

2. STUDY AREA

Uttarakhand is among the regions in the Himalayan Terrain with the most frequent earthquakes of magnitude 5.5 or higher in the past (https://asc-india.org, Gupta et al., 2012). The present study area, encompassing Rishiganga, Dhauliganga, and Girthiganga basins, Chamoli and Pithoragarh districts, Uttarakhand, covering an area of about 2800 km^2 (Figure 1)

falls in the higher Himalayas and is surrounded by a complex morphometric setup and landforms, produced by the interplay of both glacial and fluvial geomorphic processes within an active Fold-Thrust-Belt. The major part of the study area is covered by snow. The area is located within the Central Crystalline Group, which consists of Proterozoic-age rocks, including the Mana and Helang Formations. The gneiss, migmatite, schistose rocks, along with pegmatite and quartz veins prevalent in this area. Major tectonic structures like the Main Central Thrust (MCT) are indicative of the intricate structural deformation that the area has experienced. The region experiences a monsoonal climate characterized by distinct seasonal patterns. Winters are typically cold and dry, influenced by western disturbances that bring occasional snowfall, while summers are dominated by the Indian Summer Monsoon (ISM), resulting in heavy rainfall (Owen et al., 1996; Kumar et al., 2020; Kesarwani et al., 2021). This interplay of monsoonal rains and winter snowfall significantly shapes the region's cryosphere, landscape, ecosystems, and socio-economic systems (Kesarwani et al., 2021; Pandey et al., 2021). The changing climate and the continuous rise in global temperatures are expected to cause significant environmental changes, particularly in high-altitude regions of the world (IPCC, 2021). The previous studies indicate the retreatment of the Himalayan glacier due to climate change (Bajracharya et al., 2007; Kumar et al., 2020; Kesarwani et al., 2021).

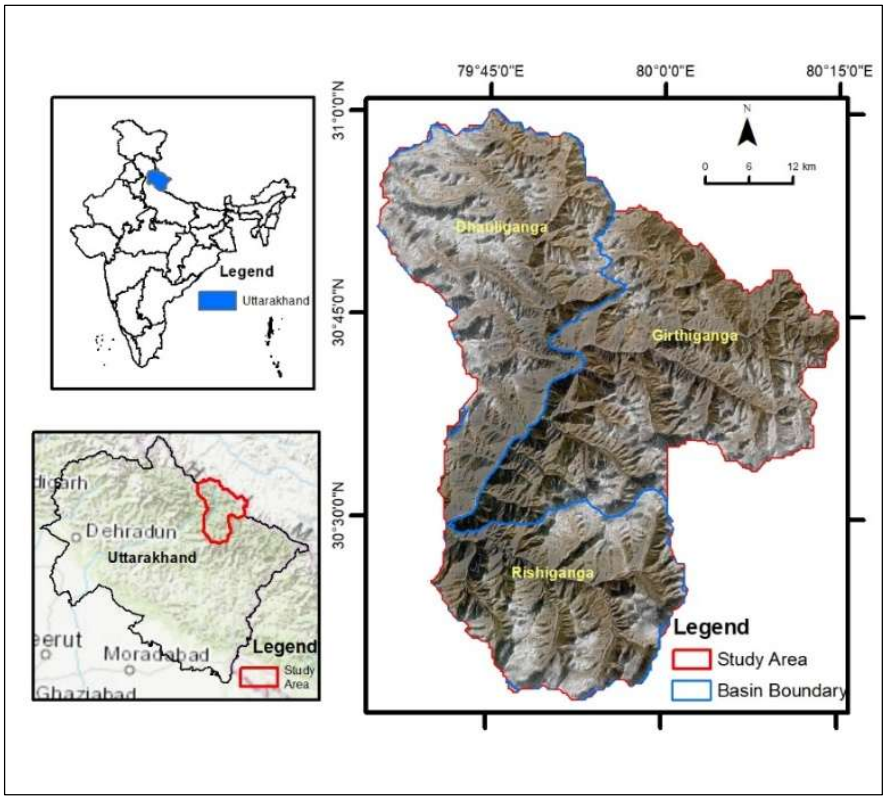

Figure 1. Location map of the study area

3. MATERIALS AND METHODOS

In this study, various optical multi-sensor and multitemporal data have been employed to create thematic maps for the multi-hazard susceptibility assessment. The details of the data products used for different thematic maps in this work are given in Table 1.

Table 1. The details of the data products used in the present study

Sl No.	Thematic maps	Data product	Source
1.	DEM derivative (Slope, Aspect, Curvature, Drainage, Landform)	ALOS PALSAR Dem (12.5m), SRTM (30 m)	Earth data, NASA, Alaska Satellite Facility - Distributed Active Archive Center
2.	Landuse Land Cover (LULC)	ASTER VNIR (15 m), LISS IV (5.8 m), Sentinel 2A (10 m)	Earth data, NASA, European Space Agency (ESA), National Remote Sensing Centre (NRSC), India
3.	Landslide Inventory	SPOT, LISS III, multitemporal Earth Observation data	NRSC, ESA, Google earth
4.	Glacier Inventory	LISS IV (5.8 m)	NRSC
5.	Earthquake Inventory	List of earthquakes	United States Geological Survey (USGS) and National Centre for Seismology (NCS)

During the present study, the multi-sensor optical data was pre-processed in Arc GIS software for the preparation of various thematic maps. The pre-processing includes layer stack, subset, calibration, and spectral enhancement of optical data. A schematic flow chart of this work is outlined in Figure 2.

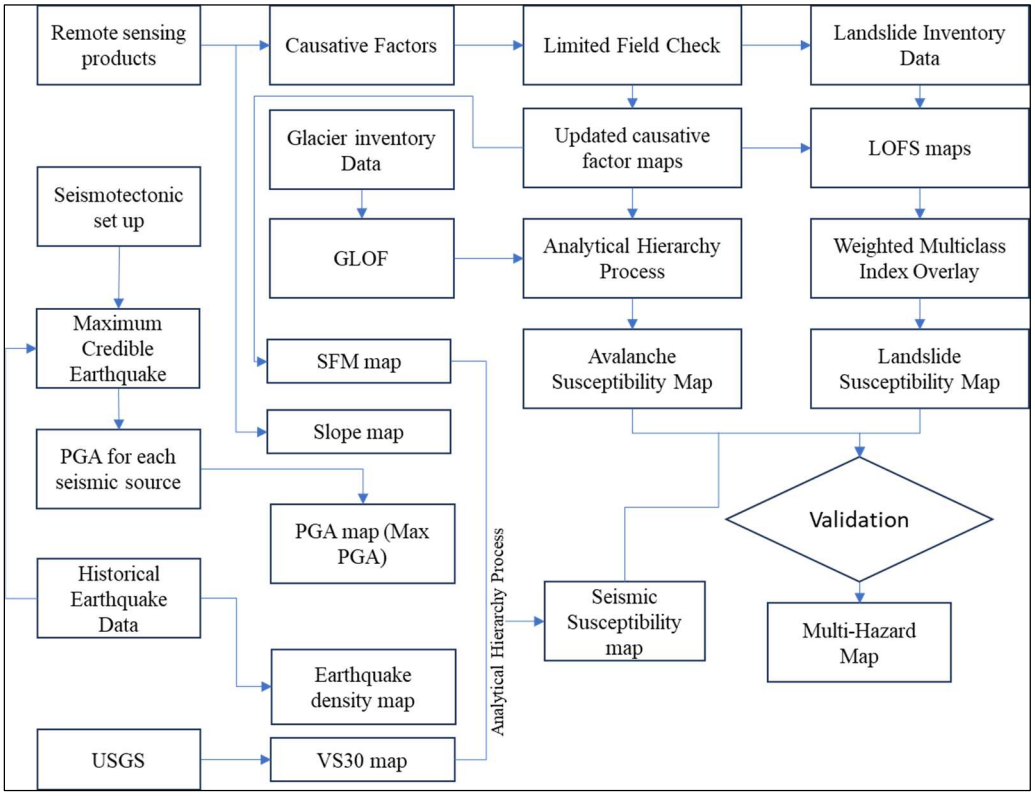

Figure 2. Methodology and workflow of the present study

3.1 Landslide Inventory

Many of the unique markers left by landslides on slopes can be recognized, categorized, and charted in the field or by photo-interpretation (Varnes, 1978; Hansen, 1984). The main way to identify these markers is through morphological changes, like variations in the slope and hummocky surfaces. By interpreting these morphological features, key landslide information can be determined, including the type of failure, the affected surface area, and the underlying

causes. The SPOT images available as a base map in Arc GIS 10.8 (up to the resolution of 30 cm), high-resolution Google Earth data of different time periods (from 2014 to 2023), and LISS III data were used as the main data product for generating the multi-temporal landslide inventory. In total, 271 landslides were digitized from remote sensing data (Figure 3). However, during the limited field check, 21 landslides were observed from the road stretch between Raini Village and Malari Village. The majority of the landslide incidences are mostly confined to the central part of the Dhauliganaga River Basin. Their occurrences in different terrain conditions are carefully studied in deriving the causative factors.

3.2 Glacier Inventory

The Himalayas have always attracted to human being for its higher mountain has unique bio-diversity with snow and ice capped peaks. It leads to increase of people activity over this region which in turn increase the fatalities as a result of avalanche incidences (Ganju et al., 2002). The assessment of the glacier and glacier lake are essential in terms of multi-hazard assessment as the avalanche as well as glacial lake outburst flood (GLOF) in the higher reaches can have domino effect in the downstream. The glaciers and glacial lakes inventory of the study area has been prepared using the multispectral IRS LISS-IV satellite images. The preparation and updating of the glacier inventory were based on the methodology outlined in the UNESCO Manual (1970) for perennial ice and snow masses, along with the guidelines provided by the Temporary Technical Secretariat (TTS) for the World Glacier Inventory, as detailed in Müller et al. (1977) and its supplement, Müller (1978). Additionally, the inventory of the Himalayan glaciers, published in GSI Special Volume No. 34 in 2009, was also referenced. A total of 204 nos. of glaciers and 97 glacial lakes have been identified. Overall, 7 vulnerable lakes have been identified across the study area (Figure 3).

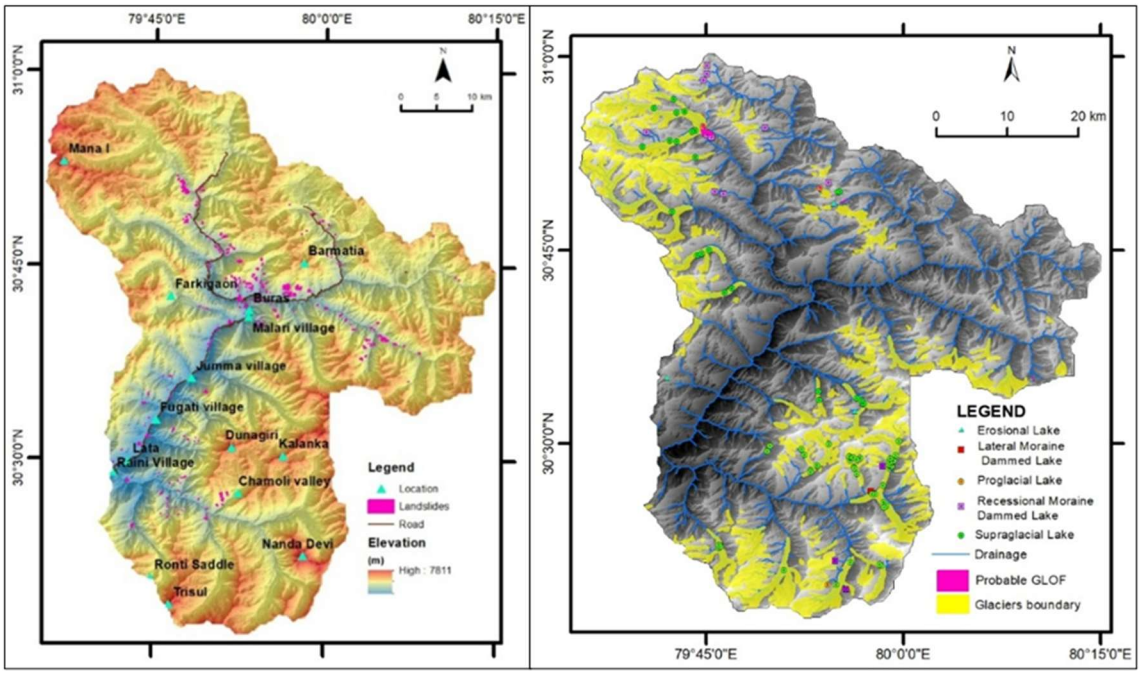

Figure 3. Spatial distribution of landslide (left) and Glacier, Glacial Lake (right) in the study area

3.3 Earthquake Inventory

The study area belongs to Seismic zone V (BIS, 2002). Although the area has not witnessed any bigger earthquake (M≥8) in the last century and is located in the Central Seismic Gap (CSG), it may experience an earthquake of higher magnitude than 8 in the future (Khattri, 1999). A seismicity analysis for an area extending 300 km from the study location has been performed using the data of earthquakes, seismic sources from the 'Bhukosh' portal of the Geological Survey of India (Figure 4). In the present study, a total of 3349 data were collected from the United States Geological Survey (USGS) and National Centre for Seismology (NCS) websites. These earthquake data have magnitude information on different scales. Thus, conversion of all the data into a uniform scale is essential. The dataset is converted into homogeneous using the following equations proposed by Das et al. (2011) and Deniz and Yucemen (2010). These empirical relationships are used by various workers in seismic studies (Sinha & Sarkar, 2020; Sharma & Sarkar, 2023).

$$Mw = 0.67(\pm 00005)Ms + 2.12(\pm 0.00001) \text{ for } 3 < M_s < 6.1 \quad (1)$$

$$Mw = 1.06(\pm 0.0002)\, Ms - 0.38(\pm 0.006) \text{ for } 6.2 \leq M_s \leq 8.4 \quad (2)$$

$$Mb = 0.65(\pm 0.003)\, Mw + 1.65(\pm 0.002) \text{ for } 2.9 \leq M_b \leq 6.5 \quad (3)$$

$$Mw = 1.57M_l - 2.66 \quad (4)$$

$$Mw = 0.54Ms + 2.81 \quad (5)$$

Where M_w = Moment magnitude, M_s = Surface wave magnitude, M_b = Body wave magnitude, M_l = Local magnitude.

Based on the completeness of the data deduced following the methodology given by Wiemer and Wyss (2000), earthquake data with magnitudes higher than 2.5 are considered for the present analysis.

3.4 Individual Hazard Assessment

In this work, due to the limitations of the data, instead of a sensu-stricto hazard assessment, susceptibility conditions with respect to landslide and avalanche have been performed. In earthquake hazard assessment, a Deterministic Seismic Hazard Analysis (DSHA) concept (Krammer, 1996; Sharma & Sarkar, 2023) has been adopted to develop the seismic micro zonation map of the area. The individual hazard assessment methodology is described below.

Landslide: The tendency of a region to produce landslides is known as its susceptibility. The landslide susceptibility is expressed mathematically as the likelihood of the slope collapse in a given location under the specific geo-environmental circumstances (Guzzetti et al., 2005). In this study, the Weighted Multi-Class Index Overlay Method was applied to map landslide

susceptibility (Guzzetti et al.,1999; Van Westen et al., 2006; Ghosh, 2011). This improved bivariate statistical method for susceptibility analysis using Yule's coefficient has been applied by many workers in the Himalayan terrain (Ghosh et al., 2011; Ram et al., 2020; Kundu & Patel, 2019; Khan et al., 2024; Bhandari & Wankhade, 2025). In this method, the interrelationship between the different classes of thematic factor (T) and landslides (L) is determined by Yule's coefficient (Y_C) by using the presence or absence of landslides in each class of the individual thematic factors. The Yc is calculated by the following equations (Yule, 1912; Fleiss, 1991; Bonham-Carter, 1994)

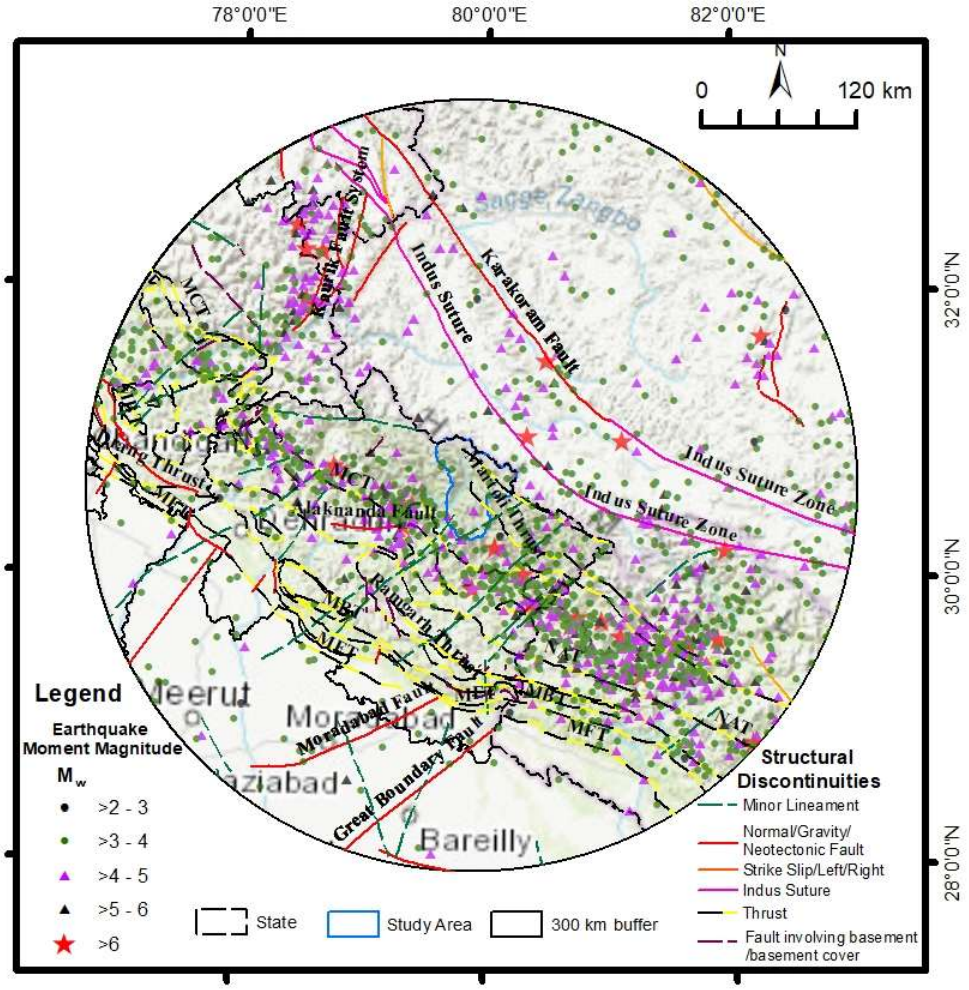

Figure 4. Seismotectonic set up of the study area showing moment magnitude of earthquake, seismic discontinuities within the 300 km radius area, MCT-Main Central Thrust, MBT-Main Boundary Thrust, MFT-Main Frontal Thrust, SAT-South Almora Thrust, NAT-Nahan Thrust

$$Y_C = \frac{\sqrt{TL/T\bar{L}} - \sqrt{T\bar{L}/TL}}{\sqrt{TL/T\bar{L}} + \sqrt{T\bar{L}/TL}} \quad (6)$$

Here, TL denotes the presence of thematic factor class as well as landslide, $T\bar{L}$ indicates absence of landslides and presence of thematic factor, $\bar{T}L$ defines the area where landslide is present, but the factor is absent, and $\bar{T}\bar{L}$ defines absence of thematic factor and landslides. The Yc is varies from -1 to + 1. A Favourability Score (FS) has been determined depending upon the value of Yc by the following equation.

$$FS = \begin{cases} 0 & for Y_C \leq 0 \\ Y_C / Y_{C_{max}} & for Y_C > 0 \end{cases} \quad (7)$$

Where, $Y_{C_{max}}$ defining the maximum Y_C of all the individual classes of the thematic factor, and FS indicates the propensity to fail for the given thematic factor.

The absolute difference of maximum Yc and minimum Yc for an individual thematic factor is taken to determine the weightage and calculated using the following equation:

$$W = |maximum\ Yc - minimumYc| / minimum|maximum\ Yc - minimumYc| \quad (8)$$

Finally, all the thematic factors are integrated based on their weightage and favourability score map using the weighted multi-class index overlay method (Bonham-Carter, 1994). Here, the susceptibility score (S) is calculated in each pixel through the following equation in the map algebra of the ArcGIS environment:

$$S = \sum_i^n (FSi \times W_i) / \sum_i^n W_i \quad (9)$$

Where FSi defines the favourability score of the ith thematic factor and Wi the weightage of the ith thematic factor.

Avalanche: Snow avalanches in the study area mostly occurred in the winter season due to heavy snowfall during this period (Ganju et al., 2002). There are various studies involving for demarcation of snow avalanche prone areas and their controlling factors in high mountain terrain (Snehmani et al., 2013; Selçuk, 2013; Kumar et al., 2016, 2019; Landrø et al., 2020; Xi & Mei, 2023). Keeping in view of the existing literature and knowledge, terrain conditions like slope, altitude, aspect, curvature, and landuse-landcover (LULC) are used in preparation of the susceptibility map. The individual subclass of each factor is given rating using the importance value scale proposed by Saaty (1980). Then, a pairwise comparison matrix is prepared, followed by a consistency check for each judgement. The consistency ratio (CR) is obtained using the following equation as proposed by Saaty (1987). It should be less than 0.1.

$$\mathrm{CR} = \frac{\mathrm{CI}}{\mathrm{RI}} \quad (10)$$

Where CI is the consistency index, and RI is the random consistency index. The Consistency Index is obtained using the following formula:

$$\mathrm{CI} = \mathrm{Mean\ CV} - \frac{\mathrm{N}}{\mathrm{N-1}} \quad (11)$$

Where mean CV is the consistency vector, and N is the order of the judgment matrix. The RI value is taken from the assigned value based on the order of the matrix (Saaty, 2000).

Now Avalanche Occurrences Favourable Score Map is obtained using the normalized fraction rating using the following formula:

$$\text{Fraction rate} = \frac{\text{Sum of each row in the judgement matrix}}{\text{no. of criteria}} \quad (12)$$

$$Avalanche\ Occurrence\ Favourability\ Score\ (AOFS) = \frac{Fraction\ Rate}{Max(Fraction\ Rate)} \quad (13)$$

The next step is to obtain the factor weight value for each thematic factor. Here also a judgment matrix needs to be prepared, followed by its consistency check, and finally, weights are calculated using the fraction rate. Now susceptibility score map is prepared by summation of the weighted AOFS map using the raster calculator in ArcGIS environment.

Earthquake: The damage due to earthquakes is the result of the collapse of infrastructures, houses, etc, due to the ground shaking. These shakings can be characterized by the Peak Ground Acceleration (Wald et al., 1999; Wu et al., 2016, 2018; Legendre et al., 2017). There are several attempts in the past for addressing this issue through the preparation of a probabilistic seismic hazard map (Khattri et al., 1984; Bhatia et al., 1999; Mahajan et al., 2010; NDMA, 2010; Kumar et al., 2011; Nath & Thingbaijam, 2012; Rout et al., 2015; Rout et al., 2018). In the present work, a deterministic seismic hazard analysis (DSHA) concept (Krammer, 1996; Sharma & Sarkar, 2023) has been adopted to prepare the seismic microzonation map of the area. The first and foremost thing for the seismic hazard analysis is the collection of past earthquake data having details of focal depth, magnitude, location, and year of occurrence.

The Maximum Credible Earthquake (MCE), the largest possible earthquake, is generally determined based on the size of the largest earthquake that is consistent with the geological, historical, and seismological data for a given region. In our study, we have estimated the subsurface rupture length distance using the following equation, as given by Wells and Coppersmith (1994):

$$\log(\mathrm{RLD}) = 0.59\mathrm{Mw} - 2.44 \tag{14}$$

Then calculate the MCE using the relationship between subsurface rupture length distance (RLD) and moment magnitude (M_w) proposed by Wells and Coppersmith (1994).

$$\mathrm{Mw}(\pm 0.28) = 5.08(\pm 0.10) + 1.16(\pm 0.07)\log(\mathrm{RLD}) \tag{15}$$

Considering the location of the study area within the CSG, probable occurrence of a major earthquake (M≥8) (Khattri, 1999; Bilham & Wallace, 2005; Bilham, 2019) and previous work (Nath et al., 2008) carried out in the Garhwal Himalaya, the MCE values for major seismic sources are taken as 8.5.

The study area has been divided into 11,334 grid points with 500 m spacing between each grid point. The MCE values derived through Eq. 6 for each seismic source is used to calculate PGA (Peak Ground Acceleration) values at each grid point using the following attenuation functions (Abrahamson & Litechiser, 1989; Mahajan et al., 2010):

$$\log 10\mathrm{av(g)} = (-1.15 + 0.245 * \mathrm{M} - 1.096\log 10(\mathrm{r} + \mathrm{e}0.256\mathrm{M}) + 0.096\mathrm{F} - 0.0011\mathrm{Er} \tag{16}$$

Where M = magnitude, r = shortest distance in kilometers from the earthquake source, ‘F’ is a dummy variable, and for reverse or reverse oblique events it is taken as 1, otherwise 0, and ‘E’ is another dummy variable and its value is taken as 1 for an interplate earthquake and 0 for

an intraplate earthquake. The max PGA value for each grid point has been taken to prepare the PGA map. Along with this PGA, based on existing literature, other factors like shear wave velocity to 30 m depth (Vs30), earthquake density, slope-forming material, and slope are considered to evaluate the seismic susceptibility map of the area using the AHP.

3.5 Causative Factor Maps

3.5.1 Topographical Parameter

Keeping in view of the existing literature and knowledge, terrain conditions like slope, altitude, aspect, curvature, drainage, and landform are used in multi-hazard study as the causative factors. The 30 m DEM data of the Shuttle Radar Topography Mission (SRTM) have been reclassified in 50 m resolution to make all the DEM derivative layers as per the 50 m x 50 m grid.

Slope: The steepness of the slope is the most significant controlling factor for avalanche initiation (Schweizer et al., 2003; Ghinoi & Chung, 2005; Kumar et al., 2016; Chen et al., 2021). The avalanche studies in the Himalaya by various authors defined the most probable slope range between 25° and 40° (Sharma & Ganju, 2000; Singh & Ganju, 2008; Snehmani et al., 2013; Kumar et al., 2017). The frequency of the landslide in general showing positive correlation with the slope gradient until it is reached in the 35°–40° class, then a negative trend is observed (Lee & Min, 2001; Dai & Lee, 2002). The slope angle map was derived from the SRTM DEM using ArcGIS 10.8. It has been reclassified into six classes for avalanche and 10 classes for landslide assessment.

Aspect: Aspect plays a key role in the stability of the snowpack (Selçuk, 2013; Kumar et al., 2016) as the sun facing area receives more solar radiation compared to the shaded area, which in turn makes the availability of a weaker layer in the shaded slope (Akbar et al., 2022). Due to the variation of the solar radiation with the aspect, the moisture retention, and vegetation also varying which in turn affects the soil strength and leads to landslides (Ullah & Zhang, 2020; Wang et al., 2020a). The slope aspect map was derived from the SRTM DEM using Arc GIS 10.8 and classified into nine classes (Figure 5) for avalanche and twelve classes for landslide assessment.

Curvature: Curvature is one of the crucial factors in avalanche initiation (Maggioni & Gruber, 2003; Snehmani et al., 2014). Several researchers have used this parameter in the assessment of avalanche susceptibility (Kumar et al., 2016,2017; Singh et al., 2018; Akbar et al., 2022). Convexity favours snow avalanche whereas concavity leads to stable slopes (Yilmaz, 2007; Nagarajan et al., 2014; Snehmani et al., 2014). The concave area tends to fail more compared to the convex area as it has high soil moisture and more surface run-off is observed within the concave area. The curvature map was derived from the SRTM DEM using ArcGIS 10.8. It has been grouped into three major classes: Flat, Concave, and Convex (Figure 5).

Altitude: Altitude has no direct influence on avalanche formation. However, with altitude, there are direct connection on temperature, wind speed, and snow formation, (Selçuk, 2013; Kumar et al., 2017). At higher elevation, snow remains available due to a drop in air temperature, whereas in the lower elevation, it melts due to higher temperature (Prasad et al., 2017). In the Himalayas, avalanche formation zones are commonly found above the tree line at altitudes exceeding 4000 meters above sea level, where the terrain is steep, and vegetation is sparse due to the high elevation (Acharya et al., 2023). However, at lower reaches around 3200 m there are also reported incidences of Avalanches in the Himalaya (Ganju et al., 2002). The altitude map was reclassified into nine classes using Arc GIS 10.8 (Figure 5).

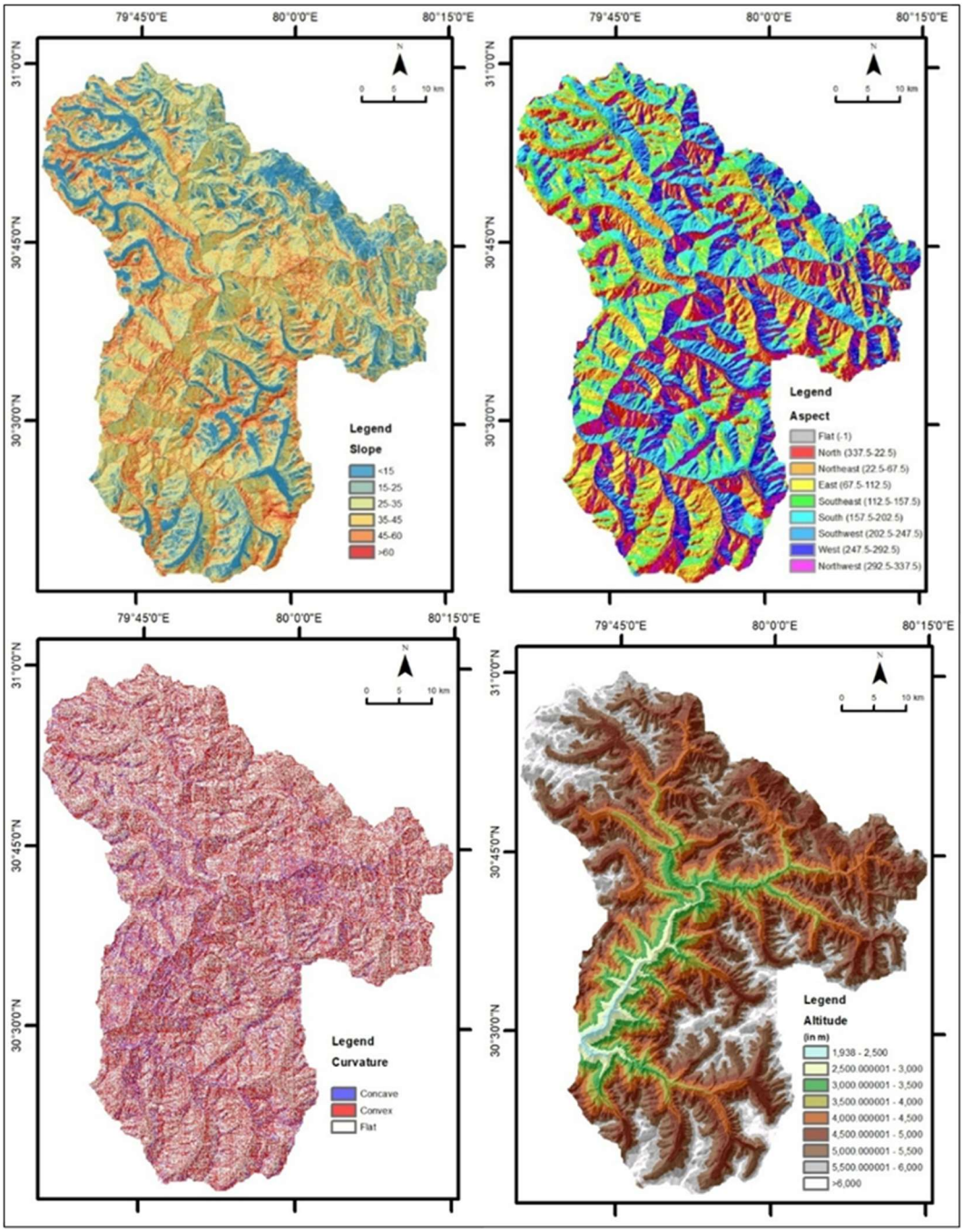

Figure 5. The causative factor slope, aspect, curvature, and altitude maps of the study area

Landform: The geomorphic form plays a significant role in slope instability, especially for slopes covered with overburden material. This form can be automatically derived from geomorphometric variables obtained from a Digital Elevation Model (Evans, 1972; Pike, 1988; MacMillan et al., 2004; Olaya, 2009). In this study, landforms were classified using the geomorphon concept (Jasiewicz & Stepinski, 2013). For the present study, landforms were derived from the SRTM DEM using this r.geomorphon script in GRASS GIS (Figure 6). It was observed that slope and hollow area show strong affinity towards landslide occurrences, followed by spur, valley, and ridge.

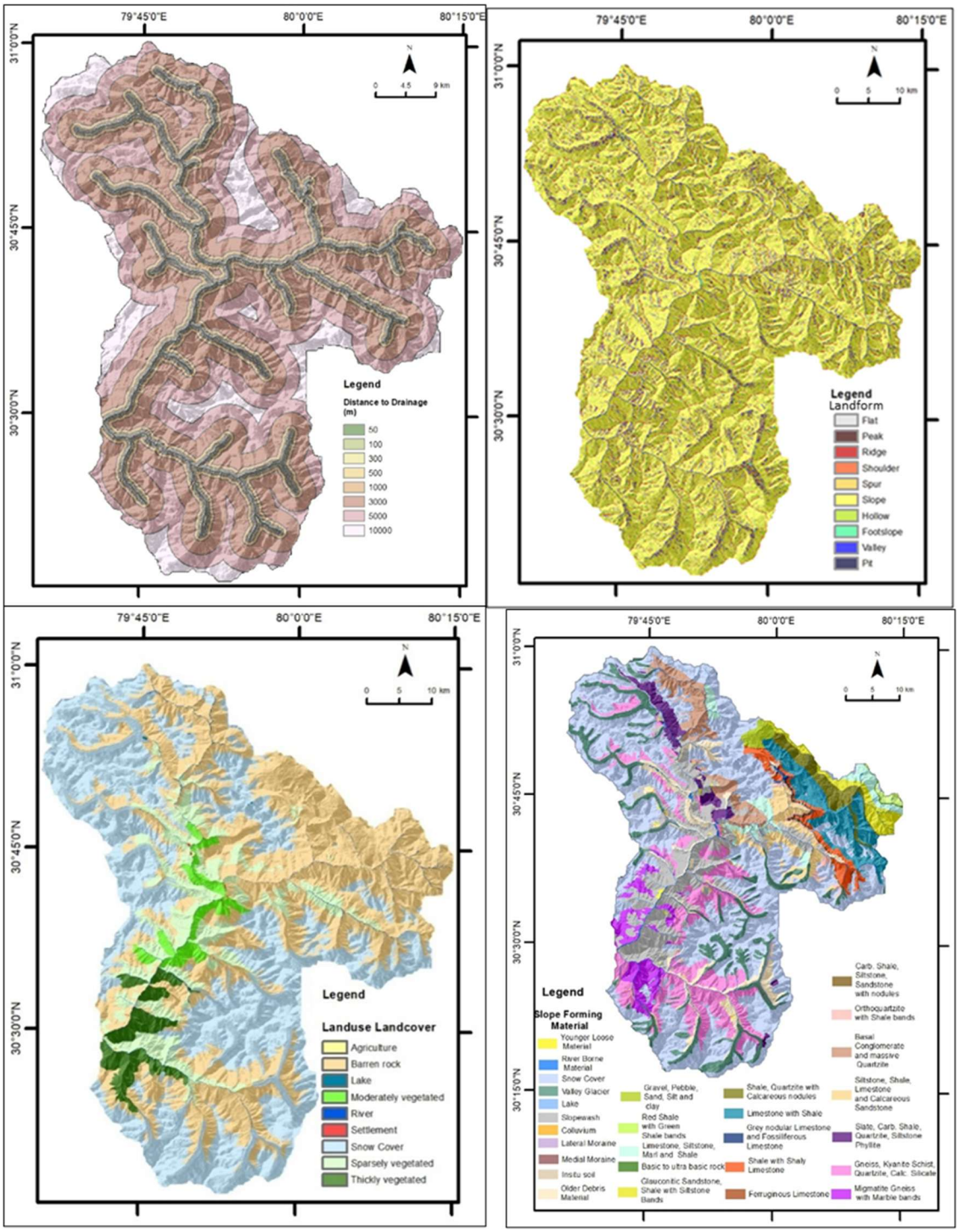

Figure 6. The causative factor distance to drainage, landform, landuse, landcover, and slope forming material maps of the study area

Drainage: Drainage also influences landslides by cutting the toe of a slope (Cevik & Topal, 2003). The drainage map study area was delineated from the SRTM DEM using the Hydrology tool of ArcGIS. In this study, 3rd order onwards drainage has been taken to calculate the multiple-ring buffer around them. The maximum distance was taken up to 10 km (Figure 6).

3.5.2 LULC

The nine land use landcover (LULC) classes have been mapped using the ASTER VNIR (15m), LISS IV (5.8m), and Sentinel 2A (10m) through band combination and Google Earth (Figure 6). Landuse landcover has control over the variability of avalanche density in the different classes (Snehmani et al., 2014; Prasad et al., 2017; Statham et al, 2018; Singh et al., 2018; Akay, 2021). For rainfall-triggered landslides the importance of LULC has been studied by various workers, having direct implications on the stability of slopes (Glade, 2003; Chen et al., 2019; Löbmann et al., 2020; Parra et al., 2021; Masi et al., 2021).

3.5.3 SFM

The slope forming material (SFM) plays a critical role in controlling the landslide occurrence. The rock-covered area of the SFM map has been prepared from the 1:50k geological map (GSI) with limited field checks. The overburden areas are demarcated using various proxies from LULC and geomorphology with limited field checks. There are thirty-five variants of slope-forming materials present across the study area (Figure 6).

3.5.4 Earthquake Density

The distribution of earthquake data indicates the level of seismic activity in the region. The higher the density, the higher the occurrence of earthquakes in the future (Ahmad & Singh, 2016). Considering the above, an earthquake density map of the area was developed using the density tool of ArcGIS. The density map has been further classified into five groups (Figure 7). There are numerous studies available on the seismic hazard assessment using the earthquake density (Soe et al., 2009; Andiana et al., 2025; Zhu et al., 2023; Malakar & Rai, 2023).

3.5.5 Vs30

Vs30 is one of the most widely used parameters for estimating shear wave velocity in sedimentary layers up to a depth of 30 meters (Chun-Hsiang et al., 2016). In tern it plays a critical factor in determining the seismic hazard of an area. Many researchers used Vs30 in evaluating the seismic hazard potential of the area, designing earthquake resistant structures (Borcherdt, 2012; Rusydi et al., 2018; Palemón-Arcos et al., 2020; Pancholi et al., 2022; Malakar et al., 2024). This work utilized the shear-wave velocity up to 30 m depth (Vs30 mosaic) developed by the United States Geological Survey (Open File Report 2007-1357, Allen & Wald, 2007). The VS30 mosaic map has been grouped into three classes: <360 m/s, >360-760 m/s, and >760 m/s (Figure 7).

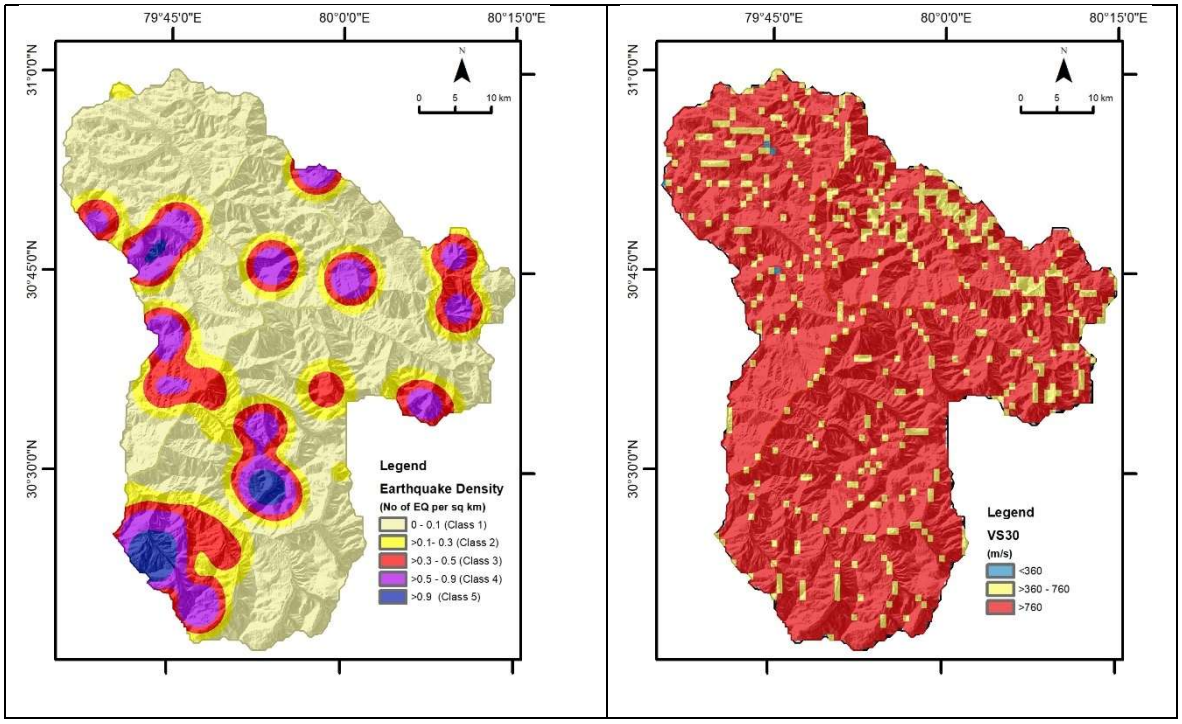

Figure 7. The causative factor earthquake density and VS30 maps of the study area

4. RESULTS

4.1 Landslide Susceptibility

The Weighted Multi-Class Index Overlay method was applied to prepare the landslide susceptibility map of the area using the seven factors. Following the methodology stated in section 3.4 and given in Figure 2, the landslide occurrence favourability score (LOFS) maps for all the causative factors were prepared. The weightage for each causative factor based on their degree of spatial association with landslides was calculated and given in Table 2. The obtained value is converted into an integer by dividing each by the maximum value. Table 2 gives the weight values of each factor map. Now using the 'map algebra' function in ArcGIS, the obtained rating maps were combined together following Eq. 9 to obtain landslide score maps. The cumulative area percentage and cumulative landslide area percentage plot is considered to classify the susceptibility map into three classes, i.e., high, moderate, and low. The value corresponds to 70% cumulative landslide percentage marks the boundary between moderate and high, whereas 90% cumulative landslide percentage marks the boundary low and moderate. Based on these cut-offs, the highly susceptible zone comprises 14 % area, containing 70% landslide, and the low susceptible zone comprises 65% area, containing 9 % landslide (Figure 8).

High susceptible zone mostly occupies along the central portion, eastern portion, south-eastern portion (Figure 8), which are highly deformed, fragile at places, and are responsible for landslide incidences. In the study area, slides observed along Raini-Malari road sector resulted from the road widening activity and the emergence of landslide incidences in the extensive

slope cutting factor class of the land-use-land-cover map. These areas have steep, barren escarpments, mostly comprising rock slides/falls.

Table 2. Weight of factor map

Factor map	Min Yc	Max Yc	Abs Diff	Weight	Integer Weight
Landform	-1.00	0.05	1.05	4.0523	4
LULC	-1	0.337272122	1.34	5.1767	5
Slope	-1.00	0.26	1.26	4.8875	5
Aspect	-0.50	0.15	0.65	2.5313	2
SFM	-1.00	0.60	1.60	6.1957	6
Curvature	-0.17	0.09	0.26	1.0000	1
Drainage	-1.00	0.58	1.58	6.1102	6

4.2 Avalanche Susceptibility

Initially, the individual classes of the causative factors have been assigned ratings based on the literature review (Snehmani et al., 2013, 2014; Kumar et al., 2017; Acharya et al., 2023). Then the AOFS value has been deduced through the judgment matrix (Table 3). After that, the weightage of each conditioning factor (Table 3) has been computed through a pairwise comparison matrix (Table 4) having the consistency index (CI) and consistency ratio (CR) of 0.04, which is acceptable. The weightage of slope factor is found to be 0.5, followed by aspect (0.25), then curvature (0.17). The weight value of altitude and LULC is 0.04, which is at the lower level of importance. Then the avalanche susceptibility has been prepared by integrating all the AOFS maps with their weightage using the following equation:

$$\mathrm{ASI} = (0.5 \times \mathrm{AOFS}_{\mathrm{Slope}} + 0.25 \times \mathrm{AOFS}_{\mathrm{Aspect}} + 0.17 \times \mathrm{AOFS}_{\mathrm{Curvature}} + 0.04 \times \mathrm{AOFS}_{\mathrm{Altitude}} + 0.04 \times \mathrm{AOFS}_{\mathrm{LULC}}) \quad (17)$$

The output map has been classified into three classes, namely low, covering about 45% of the area, moderate, covering about 26% of the area, and high, covering about 29 % of the area (Figure 8). Out of the 204 glaciers, 31 glaciers encompass more than 50% high susceptible area.

4.3 Earthquake Susceptibility

Assessing seismic hazard involves estimating the ground motion likely to occur at the site of interest. Attenuation relationships represent the most widely used approach in engineering to estimate ground motion. In this work, the Ground Motion Prediction Equation (GMPEs), i.e., the attenuation function given in Eq.16, is used to estimate the expected PGA for each grid cell. Distance to source and source characteristics are the key elements in deriving the PGA using the attenuation relationship. In this context, the type of fault, i.e., thrust, strike-slip, or normal faults, is noted and shortest distance parameter in each grid cell for each source is calculated. The PGA values vary from 0.14 g to 0.98 g. The PGA has been calculated at the bedrock level. It can be amplified within the overburden-covered area depending upon the characteristics of the overburden material. The PGA map has been classified into four classes, namely low having PGA value <0.24g, moderate with PGA ranging from 0.24g to 0.36g, high with PGA varying from 0.36-0.6g, and very high having more than 0.6g (Figure 8). Along with

this PGA map, based on the literature study, SFM, VS30, earthquake density, and slope maps are incorporated in the evaluation of the earthquake susceptibility. Saaty's Analytical Hierarchy Process is utilized to derive the weightage of the thematic factors and individual classes of the themes. A pairwise judgement matrix is given in Table 5. The earthquake hazard of the area is obtained through the weighted integration of all the thematic factors. The map is classified into three classes: low, moderate, and high using the natural break criterion. The low, moderate, and high susceptibility area cover 49%, 30%, and 21% of the total area, respectively (Figure 8). High susceptibility area is mainly located in the central, southeastern, and southwestern regions.

Table 3. The assigned ratings for individual classes of conditioning factors

Conditioning Factor	Categories	Rating	AOFS	Consistency Ratio	Weight
Slope	<15	1	0.0663	0.04	0.5
	15-25	3	0.1516		
	25-35	6	0.4461		
	35-45	9	1.0000		
	45-60	4	0.2281		
	>60	2	0.0989		
Aspect	N	9	1.0000	0.04	0.25
	NE	5	0.2712		
	E	3	0.1304		
	SE	7	0.5092		
	S	2	0.0897		
	SW	8	0.7097		
	W	1	0.0641		
	NW	4	0.1895		
	Flat	0	0		
Curvature	Concave	2	0.1431	0.03	0.17
	Flat	3	0.2410		
	Convex	7	1.0000		
Altitude	1938-2500 m	1	0.0692	0.04	0.04
	2501-3000 m	2	0.1010		
	3001 - 3500 m	3	0.1544		
	3501 - 4000 m	4	0.2497		
	4001 - 4500 m	7	0.5697		
	4501 - 5000 m	9	1.0000		
	5001 - 5500 m	9	1.0000		
	5500 - 6000 m	4	0.2308		
	>6000 m	2	0.1010		
LULC	Barren	3	0.3090	0.01	0.04
	Snow Cover	7	1.0000		
	Agricultural	2	0.1859		
	Sparse Vegetation	2	0.1859		
	Moderate Vegetation	1	0.1066		
	Thick Vegetation	1	0.1066		
	Settlement	0	0		
	Lake	0	0		
	River	0	0		

Table 4. Pairwise judgement matrix of the conditioning factors

Factor	Slope	Aspect	Altitude	LULC	Curvature	Weight
Slope	1.00	3.00	7.00	8.00	4.00	0.5
Aspect	0.33	1.00	5.00	6.00	2.00	0.25
Altitude	0.14	0.20	1.00	2.00	0.25	0.04
LULC	0.13	0.17	0.50	1.00	0.20	0.04
Curvature	0.25	0.50	4.00	5.00	1.00	0.17

Table 5. Pairwise judgement matrix of the thematic factors

Factor	SFM	PGA	VS30	Density	Slope	Weight	Consistency Ratio
SFM	1.00	0.33	0.50	0.25	4.00	0.12	0.03
PGA	3.00	1.00	2.00	0.50	6.00	0.28	
VS30	2.00	0.50	1.00	0.33	5.00	0.16	
Density	4.00	2.00	3.00	1.00	7.00	0.4	
Slope	0.25	0.17	0.20	0.14	1.00	0.04	

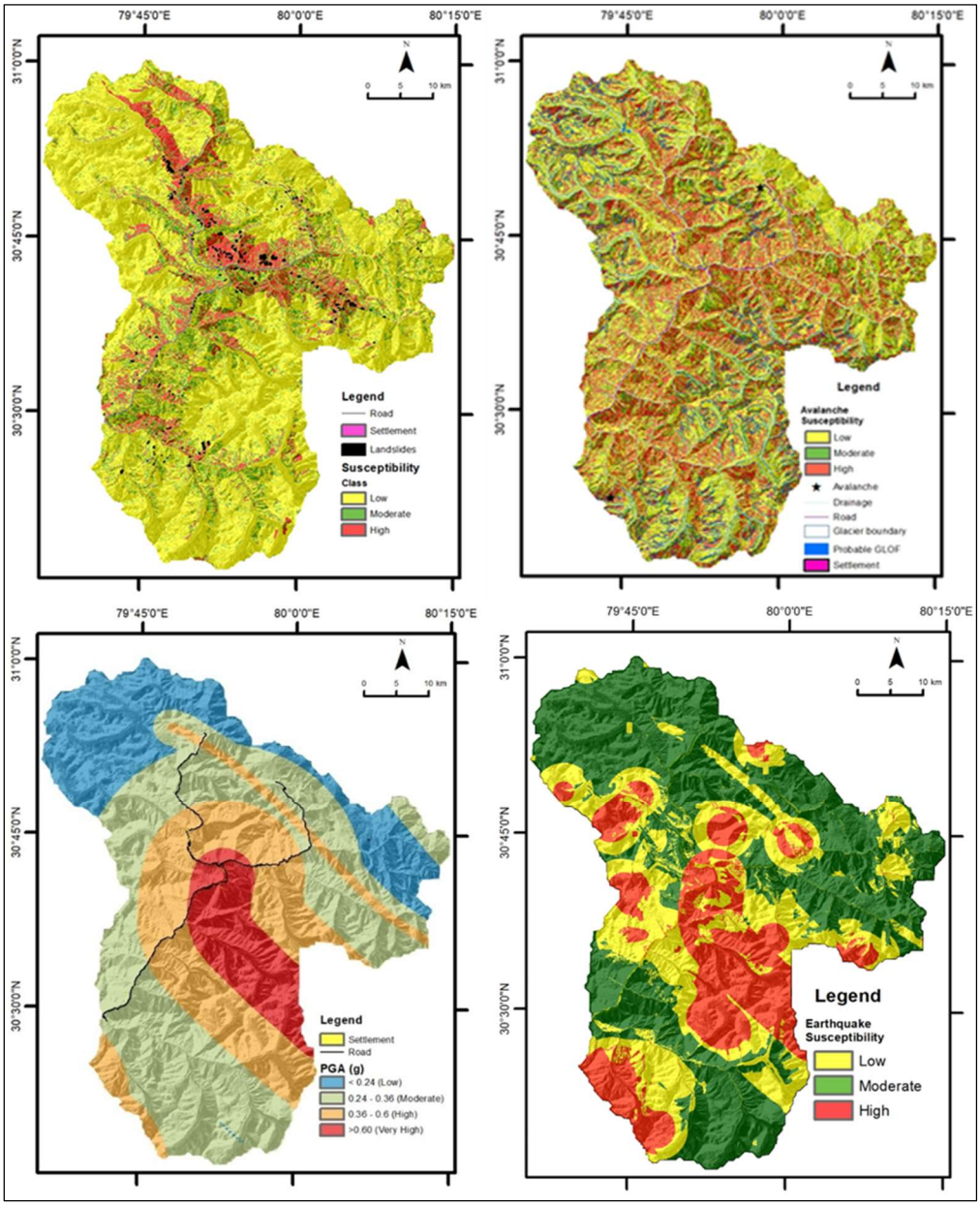

Figure 8. Landslide susceptibility map (top left), Avalanche susceptibility map (top right), PGA map (bottom left), Earthquake susceptibility map (bottom right)

4.4 Multi-Hazard

In this work, a straightforward multi-hazard assessment has been performed by combining the three hazards. The combined map represents the likelihood occurrence of single hazard types (Landslide-LS, Earthquake-EQ, and Snow avalanche-AVA) and their combined occurrence (LS+EQ+AVA, LS+EQ, LS+AVA, and EQ+AVA). The combined map was reclassified based on the presence or absence of moderate and high classes of individual susceptibility maps. The proposed classification schema is shown in Table 6. Figure 9 shows the multiple-hazard map of the study area. It shows that about 16% of the study area is located within a low hazard zone, the hazard zone for single hazard type covers 17% (Avalanche), 17% (Earthquake), and 4% (Landslide) of the study area. Whereas around 46% of the study area is affected by multiple hazard types. In consideration of the presence of individual susceptibility classes, the multi-hazard map has been further reclassified into four classes: low, moderate, high, and very high (Table 6, Figure 9). The low, moderate, high, and very high hazard areas occupy about 18%, 40%, 31%, and 11% of the study area, respectively.

Table 6. Classification schema of susceptibility models

Sr No	Earthquake Susceptibility	Avalanche Susceptibility	Landslide Susceptibility	Multi Hazard	Multi Hazard Class
1	Low	High	Moderate	AVALS	High
2	Low	Moderate	Low	AVA	Moderate
3	Low	Low	Moderate	LS	Moderate
4	Low	High	High	AVALS	Very High
5	Low	Low	Low	Low	Low
6	Low	Moderate	Moderate	AVALS	Moderate
7	Low	High	Low	AVA	High
8	Low	Low	High	LS	High
9	Moderate	Low	Low	EQ	Moderate
10	Moderate	Moderate	Low	AVAEQ	Moderate
11	Low	Moderate	High	AVALS	High
12	Moderate	High	Low	AVAEQ	High
13	Moderate	High	Moderate	AVAEQLS	High
14	Moderate	Moderate	Moderate	AVAEQLS	Moderate
15	Moderate	Low	Moderate	EQLS	Moderate
16	Moderate	High	High	AVAEQLS	Very High
17	Moderate	Moderate	High	AVAEQLS	High
18	Moderate	Low	High	EQLS	High
19	High	Moderate	Moderate	AVAEQLS	High
20	High	Moderate	Low	AVAEQ	High
21	High	Low	Low	EQ	High
22	High	High	Low	AVAEQ	Very High
23	High	Low	Moderate	EQLS	High
24	High	High	Moderate	AVAEQLS	Very High
25	High	High	High	AVAEQLS	Very High
26	High	Low	High	EQLS	Very High
27	High	Moderate	High	AVAEQLS	Very High

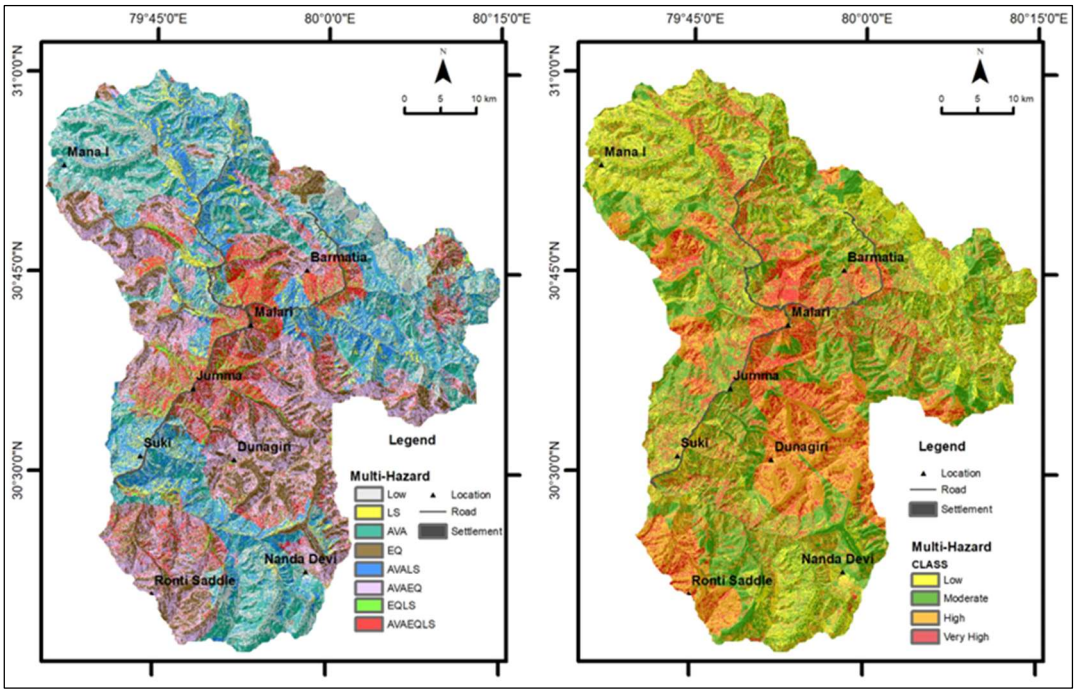

Figure 9. Multiple hazard map (left) showing combination of three hazard maps (LS -Landslides, EQ-Earthquake, AVA-Avalanche) and (right) showing distribution of multi-hazard classes

4.5 Validation

In the scientific community, a model is considered unacceptable without proper validation (Wubalem & Meten, 2020). In this work, in order to check the performance, and accuracy of the individual susceptibility models, the area under the receiver operating curve (AUROC) and statistical indices like Sensitivity, Specificity, Accuracy, Positive Predictive Value (PPV), Negative Predictive Value (NPV), and Cohen's Kappa values are used. These validation techniques have been used by many researchers following the standard definition of the statistical indices (Düntsch & Gediga, 2019; Dou et al., 2020; Gupta et al., 2024; Abdelkader & Csámer, 2025; Chauhan et al., 2025).

The landslide model shows an AUC of 0.87 (Figure 10), which is a very good performance (Özay & Orhan, 2023), and the earthquake susceptibility model shows an AUC of 0.79 (Figure 10) + revealing good performance (Özay & Orhan, 2023). Further, various statistical indices are evaluated to see the model efficacy and are given in Table 7. The accuracy of landslide and earthquake susceptibility models was determined to be 83% and 85%, respectively. The Kappa values of both the susceptibility models (earthquake and landslide) show substantial agreement between the models.

Table 7. Statical indices for susceptibility map validation

Map	Model	Accuracy	Sensitivity	Specificity	PPV	NPV	Kapp Value
Landslide Susceptibility	Multiclass Index Overlay	0.83	0.77	0.85	0.73	0.88	0.62
Earthquake Susceptibility	AHP	0.85	0.83	0.86	0.93	0.67	0.63

The recent two incidents of avalanches in the study area fall within the highly susceptible zone, which validates the model.

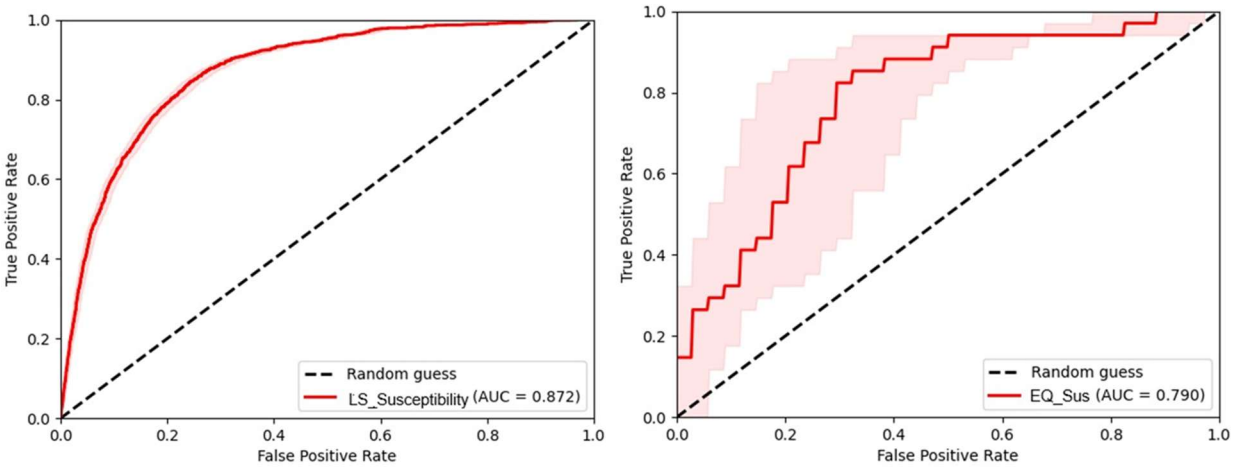

Figure 10. ROC curve and AUC values showing performance of the models-Landslide (left) and earthquake (right)

5. DISCUSSION

Multi-hazard analysis involves understanding the interplay between different hazards, their likelihood, and the potential cascading effects. This analysis can help design mitigation strategies, improve disaster preparedness, and prioritize actions based on vulnerability and risk. Sometimes a single natural event can trigger or elevate the likelihood of one or more other natural hazards occurring (Jinxing et al., 2002; Bathrellos et al., 2017; Hagenlocher et al., 2018). The present study in the Rishiganga and Dhauliganga basin of Chamoli district, Uttarakhand focus on the demarcation of susceptible areas for the natural hazards in terms of snow avalanches, landslides, and earthquakes and their interactions, providing insights into the cumulative risks faced by the region's communities and infrastructure. The area is inaccessible and falls in the permafrost region. In this work, an innovative approach has been attempted in such inaccessible and permafrost terrain using multisensory and temporal earth observation data with limited field check for a multi-hazard zonation study. Based on the literature review and site conditions, different thematic factors are considered for the assessment of individual hazards. Multi class index overlay method was used for landslide, whereas AHP was used for earthquake and avalanche hazards. There are previous works on the integration of the high to very high susceptible area for all the hazard types to define the high hazard zone and the rest is a low category (Pourghasemi et al., 2019, 2020; Yousefi et al., 2020; Rusk et al., 2022). This categorization of the susceptibility zone into two classes simplifies the integration process of different hazard types. However, the moderate category, which is also susceptible to natural hazards covering a good portion of the investigated area, is ignored in this grouping. Researchers also used AHP in delineating the weightage of the individual hazard types to develop the multi-hazard map (Bathrellos et al., 2017; Skilodimou et al., 2019). But it requires adequate data input on the past records of various hazards to provide a reliable weightage. Moreover, for a given area some parts are more susceptible with respect to a specific natural

hazard compared to others. Thus, a higher weightage for a single hazard type to delineate the multi-hazard map of the whole area will not bring the actual picture of the multi-hazard scenario of the region. Sharma and Rana (2024) evaluate the weight considering the hazard frequency, damage data, and ground survey. In a similar way, Sharma et al. (2024) also estimate the weightage of the individual hazard types to assess the multi-hazard risk of the Jammu region. Due to a lack of sufficient past hazard data and to overcome the above difficulties in multiple hazard integration, a simple classification schema for the hazard integration is proposed (Table 6). Here, moderate and higher classes are taken into consideration to assign the hazard types.

The analysis of landslide susceptibility indicates the occurrence of high susceptible zone mainly in the central region, along the road corridors and valleys in northern, southern, and eastern part where steep slopes, highly deformed and fragile rock mass at places is present. These areas have witnessed numerous landslide incidents in the past. These landslides occurred from the interplay of slope shape, rock mass characteristics, along with surface and groundwater movements, which corroborates the study of Bogaard and Greco (2016). The landslide susceptible zones are identified by the Weighted Multiclass Index Overlay Method using the seven thematic factors viz., Slope, Aspect, Curvature, Drainage, Landform, LULC, and SFM. Besides, other contributing elements like rainfall, seismic activity, snowmelt, or human actions can also trigger hazardous landslides (Petley, 2012; Haque et al., 2019). Due to the non-availability of rainfall data and its dynamic nature, this factor is not considered in the present work. Similarly, considering the dynamic nature of seismic activity, snow melt, they are also not included. However, while demarcating a multi-hazard scenario, the probable occurrence of avalanche as well as earthquake in the landslide-prone area is considered in order to reflect the zone of multiple hazard interaction area. About 14 % of macro scale susceptibility maps are grouped under the high susceptibility class, whereas the moderate susceptibility zone covers 21 %, and the low susceptibility class covers 65 % of the study area. The landslide susceptibility assessment is crucial in this terrain as it aids in estimating the impact of future landslides, and can be used to locate the safe road alignment, vital infrastructure like hospitals, fire stations, etc. Public or private utility projects should be avoided in highly susceptible areas. However, the susceptibility values can be lowered if proper mitigation measures are adopted, such that a highly susceptible area can be made less vulnerable to landslides.

A major part of the study area is covered by snow (Figure 6). In the Indian Himalayas, about three-quarters of fatalities are due to snow avalanches and extreme climatic conditions (Kumar et al., 2017). It is commonly believed that future avalanche events will primarily occur in areas where avalanches have been previously documented (Hebertson & Jenkins, 2003). However, due to the remote accessibility, the documented avalanches are poor in many areas. In this case topographical parameters are used to assess the avalanche-prone zone (Eckert et al. 2007a, b; Maggioni & Gruber, 2003). In line with the above, in this present work, the layers were prioritized based on a review of relevant literature and field observations. The AHP (Analytic Hierarchy Process) method of multi-criteria decision-making (MCDM) analysis was used in evaluating the avalanche susceptibility condition of the area (Snehmani et al., 2014; Kumar et al., 2016; Singh et al., 2018; Rafique et al., 2023; Xi & Mei, 2023). The avalanche susceptibility map reveals that low susceptible covering about 45%, moderate about 26%, and high about

26 % of the area. The high susceptible area is mostly located in the steep snow-covered area. Avalanche initiation due to the steepness of the slope was also mentioned in earlier studies carried out by various researchers (Sharma & Ganju, 2000; Singh & Ganju, 2008; Ancey, 2013; Snehmani et al., 2013; Kumar et al., 2017). Two recent avalanche occurrences, one in the southern part of the Rishiganga avalanche that occurred during February 2021, and the other in the northern part that occurred in April 2021, are located within the highly susceptible zone (Fig.8). The road passes through 26% high susceptible, 22% moderate, and 52% low susceptible areas. It has been found that 31 glaciers out of 203 glaciers encompass more than 50% high susceptible area. Thus, an avalanche due to the high snowfall may lead to a sudden flood in these valleys. Moreover, melting of these glaciers can also trigger floods and may affect the downstream areas. Within the glacierized regions, a total of 97 glacial lakes have been identified, and among these, 7 lakes are vulnerable (Probable GLOF area).

Seismic hazard analysis (SHA) involves evaluating the potential seismic risk in a region, typically expressed in terms of Peak Ground Acceleration (PGA). PGA is a critical parameter in earthquake engineering for assessing the level of shaking a structure might experience. The higher the PGA, the greater the potential damage to structures due to ground shaking. Some of the key seismic sources in this area are MCT, MBT, HFT, NAT, SAT, Martoli Thrust, Kaurik Fault, Karakoram Fault, and Indus Suture Zone. Considering the historical earthquake data and regional tectonic setting, the maximum credible earthquake i.e., the worst-case scenario with respect to each seismic source are determined. The estimation of PGA is done by the empirical models of ground motion prediction equations using the seismic source parameters. The resulting PGA values are at higher side compared to other works (Nath & Thingbaijam, 2012; Rout et al., 2015, 2018; Sharma & Sarkar, 2023). The variation is mainly due to the consideration of different MCE conditions during this work. Although the MCE derived using the empirical formula (Wells & Coppersmith, 1994) is varying from 5.67 to 7.04 M_w, the MCE value is taken as 8.5 for the northerly dipping major thrust categories based on the estimation of probable earthquake occurrence with magnitude ≥8 (Khattri, 1999; Bilham & Wallace, 2005; Nath et al., 2008; Bilham, 2019) and location of the area well within the Central Seismic Gap of Himalaya. The earthquake susceptible zone was delineated using the AHP method encompassing PGA, Earthquake density, VS30, Slope, and SFM maps. The analysis demarcated the presence of a high susceptible zone in the central, southeastern, and southwestern parts of the area. These localities experienced previous earthquake events and situated in the high PGA zone, low VS30 area, and some part in overburden covered area. It is pertinent to mention that there was no reported work in developing the earthquake susceptible map using the PGA, and VS30 for the study area. Mainly, they defined the seismic hazard potential in terms of PGA (Nath & Thingbaijam, 2012; Sharma & Sarkar, 2023). Buildings in the high zones need to be designed with reinforced materials and earthquake-resistant techniques. These areas may have building codes that require stricter regulations, while less affected areas may have more lenient codes. This earthquake susceptibility map can help the local governments and organizations in emergency response planning and mitigation measures.

The combined tool of the ArcGIS platform was applied in the integration of the three susceptibility maps (Avalanche, Earthquake, and Landslide) to prepare the multi-hazard map.

The output map was reclassified as per the proposed criterion given in Table 6. The multi-hazard map grouped the area into single hazard prone area (Avalanche-17%, Earthquake-17%, Landslide-04%), multiple hazard prone area (two or more, 46%), and the rest (16%) as low (Figure 9). Further, it has been reclassified into four classes considering the susceptibility level of each hazard type with the area covered by the low, moderate, high, and very high hazard for about 16%, 36%, 35%, and 13% respectively (Figure 9). The former map delineating the individual hazard zone as well as multiple hazard areas, in conjunction with the low to very high classified map, will be very helpful in understanding the interaction zone of one hazard with the other and its final hazard category in order to planning effecting mitigation strategy and resource allocation.

The future work may be conducted on more detailed manner by incorporating site response in characterizing earthquake causative factors, consideration of additional parameters for landslide and avalanche assessment through adequate ground survey, which are the limitations of the present work. Besides, the machine learning method is also not conducted due to a lack of sufficient inventory of individual hazard categories.

6. CONCLUSION

The area is prone to various natural hazards as witnessed in other parts of the Himalayan region (Gautam et al., 2013; Kala, 2014; Pathak et al., 2019). The present remote sensing-based study of all the thematic layers with limited field checks and modelling of the multi-hazards will be very useful in the policy and planning for the preparedness for all sorts of infrastructure projects, mitigation, and management for rescue and rehabilitation of the flood and hazard-affected areas. The novel approach introduced in this work in delineating the area in different zones, either by single hazard type or by multiple hazards, will help the planners in developing suitable mitigation strategies depending on the hazard types.

The identified vulnerable lakes in both basins need to be regularly monitored to avoid GLOF hazards in this area. A similar methodology may be adopted in other inaccessible parts of the Higher Himalayas for multi-hazards zonation study.

The macroscale susceptibility map provides valuable inputs for specific land use and urban planning. However, it is advised that a thorough site-specific analysis be carried out prior to the planning and implementation of the civil construction projects. When carrying out civil works, areas that are susceptible to significant hazards should receive the attention they require.

Spatio-temporal prediction of multi-hazard is still difficult on the macro-scale; hence, questions can be raised about the predictive capability of a susceptibility map given the uncertainty in the occurrence of a single or combined hazard.

If buildings are not positioned safely and appropriately, the loss in the case of a disaster would be enormous. Raising awareness is the most cost-effective strategy to reduce the loss of

life and property. As a result, it is advised that the Community-Based Disaster Management Program (CBDMP) be given more importance

Information on the possible threat, how to recognize and communicate it, the physical significance of the hazard and its inherent uncertainties, strategies to lower the risk of multi-hazards, and local mitigation measures should all be included in the awareness.

REFERENCES

Abdelkader, M.M., & Csámer, Á. Comparative assessment of machine learning models for landslide susceptibility mapping: a focus on validation and accuracy. *Natural Hazards, 121*, 10299–10321 (2025). https://doi.org/10.1007/s11069-025-07197-0

Abrahamson, N. A., & Litcheister, J. J., (1989), Attenuation of vertical peak acceleration, *Bulletin of the Seismological Society of America, 79*, 549-580

Acharya, A., Steiner, J.F., Walizada, K.M., Zakir, Z.K., Ali, S., Caiserman, A, & Watanabe, T., (2023), Review article: Snow and ice avalanches in high mountain Asia –scientific, local and indigenous knowledge. *Natural Hazards and Earth System Sciences*, *23*, 2569–2592, https://doi.org/10.5194/nhess-23-2569-2023, 2023.

Akay, H. (2021). Spatial modeling of snow avalanche susceptibility using hybrid and ensemble machine learning techniques. *CATENA*, *206*,2021, 105524

Akbar, M., Bhat, M.S., Chanda, A., Lone, F.A., & Thoker, I.A., (2022), Integrating Traditional Knowledge with GIS for Snow Avalanche Susceptibility Mapping in Kargil-Ladakh Region of Trans-Himalayan India. *Spatial Information Research, 30*, 773–789

Akbar, M., Bhat, M.S., & Khan, A.A. (2023). Multi-hazard susceptibility mapping for disaster risk reduction in Kargil-Ladakh region of Trans-Himalayan India. *Environmental Earth Sciences*, *82* (2), 68. doi:10.1007/s12665-022-10729-7

Aksha, S. K., Resler, L. M., Juran, L., & Carstensen, L. W. (2020). A geospatial analysis of multi-hazard risk in Dharan, Nepal. Geomatics, *Natural Hazards and Risk*, *11*(1), 88–111. https://doi.org/10.1080/19475705.2019.1710580

Ali, N., Alam, A., Bhat, M.S., & Shah, B. (2022). Using historical data for developing a hazard and disaster profile of the Kashmir valley for the period 1900–2020. *Natural Hazards, 114*, 1609–1646. https://doi.org/10.1007/s11069-022-05440-6

Allen, T.I., & Wald, D.J. (2007). Topographic Slope as a Proxy for Seismic Site-Conditions (VS 30) and Amplification Around the Globe. *United States Geological Survey*, *Open-File Report 2007-1357*,69

Ancey, C. (2013). Snow Avalanches. In B. Schrefler & P. Delage (Eds.), *Environmental Geomechanics*, New York, 2013.

Andiana SA, Samodra, SB, & Wibowo, NB. (2025). Microzonation of Earthquake Hazard Using Analytical Hierarchy Process (AHP) in The Sri Gethuk Waterfall Tourist Area and Surroundings, Playen and Dlingo Subdistrict, Special Region of Yogyakarta, *IOP Conference Series.: Earth and Environmental Science*, 1517 012013

Bajracharya, S.R., Mool, P.K., & Shrestha, B.R., 2007. Impact of Climate Change on Himalayan Glaciers and Glacial Lakes: Case Studies on GLOF and Associated Hazards in

Nepal and Bhutan. *International Centre for Integrated Mountain Development (ICIMOD),* Kathmandu (Publication, 119)

Baruah, S., D'Amico, S., Saikia, S., Gautam, J. L., Mrinalinee Devi, R. K., Boruah, G. K., Sharma, A., Abdelwahed, M. F. (2018). Study of fault plane solutions and stress drop using local broadband network data: The 2011 Sikkim Himalaya earthquake of Mw 6.9 and its aftershocks. *Annals of Geophysics, 61*(1), SE107. https://doi.org/10.4401/ag-7367

Bathrellos, G. D., Skilodimou, H. D., Chousianitis, K., Youssef, A. M., & Pradhan, B. (2017). Suitability estimation for urban development using multi-hazard assessment map. *Science of The Total Environment, 575*, 119–134

Bhandari, A. N., & Wankhade, H. L. (2025). Bivariate landslide susceptibility analysis for parts of Kumaon Himalayas: A case study of Nainital town and its surroundings, India. *Natural Hazards Research, 5(3)*, 481–494. https://doi.org/10.1016/j.nhres.2025.01.001

Bhatia S C, Kumar M R & Gupta H K., (1999), A probabilistic seismic hazard map of India and adjoining regions; *Annals of Geophysics, 42,* 1153–1164, https://doi.org/10.4401/ag-3777

Bilham, R., & Wallace, K. (2005). Future Mw>8 earthquakes in the Himalaya: implications from the 26 Dec 2004 Mw=9.0 earthquake on India's eastern plate margin. *Geological Survey of India Special Publication, 85*, 1-14

Bilham, R., (2019), Himalayan earthquakes: a review of historical seismicity and early 21st century slip potential. TRELOAR, P. J. & SEARLE, M. P. (eds) 2019. Himalayan Tectonics: A Modern Synthesis. *Geological Society, London, Special Publications*, *483*, 423–482

Bogaard, T.A., & Greco, R. (2016). Landslide hydrology: from hydrology to pore pressure. *Wires. Water,* 3, 439–459. https:// doi. org/ 10. 1002/wat2. 1126

Bonham-Carter, G.F. (1994). Geographic Information Systems for Geoscientists: Modeling with GIS. *Computer Methods in the Geosciences, 13, Pergamon*, *Elsevier Science Limited*., 398

Borcherdt, R. (2012). Vs30–A site-characterization parameter for use in building codes, simplified earthquake resistant design, GMPEs, and ShakeMaps. *In: Proceedings of fifteen World Conference on Earthquake Engineering, Lisbon, Portugal, September 24-28, 10*

Çevik, E., & Topal, T. (2003). GIS-based landslide susceptibility mapping for a problematic segment of the natural gas pipeline, Hendek (Turkey). *Environmental Geology, 44*, 949–962. https://doi.org/10.1007/s00254-003-0838-6

Chauhan, V., Gupta, L., & Dixit, J. (2025). Machine learning and GIS-based multi-hazard risk modeling for Uttarakhand: Integrating seismic, landslide, and flood susceptibility with socioeconomic vulnerability, *Environmental and Sustainability Indicators*, *26,* 100664, ISSN 2665-9727, https://doi.org/10.1016/j.indic.2025.100664.

Chen L, Guo Z, Yin K, Shrestha, D.P, & Jin, S. (2019), The influence of land use and land cover change on landslide susceptibility: a case study in Zhushan Town, Xuan'en County (Hubei, China). *Natural Hazards and Earth System Sciences, 19*,2207–2228. https:// doi. org/ 10. 5194/ nhess- 19- 2207- 2019

Chen, Y., Chen, W., Rahmati, O., Falah, F., Kulakowski, D., Lee, S., Rezaie, F., Panahi, M., Bahmani, A., Darabi, H., Ali, T.H., & Bian, H. (2021). Toward the development of deep-

learning analyses for snow avalanche releases in Mountain regions. *Geocarto International, 37*, 1-25.

Chouhan, S., Narang, A., & Mukherjee, M. (2022a). Multi-Hazard Risk Assessment of Schools in Lower Himalayas: Haridwar District, Uttarakhand, India, *European Geosciences Union General Assembly* 2022, Vienna, Austria, 23–27 May 2022, EGU22-4333, https://doi.org/10.5194/egusphere-egu22-4333

Cruden DM, & Varnes DJ. (1996). Landslide types and processes. *In: Turner AK, Shuster RL (eds) Landslides: investigation and mitigation. Special Report, 247, Transportation Research Board, National Academy of Sciences,* Washington, D.C 36–75

Dai F.C. & Lee C.F. (2002). Landslide characteristics and slope instability modelling using GIS, Lantau Island, Hong Kong. *Geomorphology, 42*, 213– 228

Das R, Wason, H. R., & Sharma M. L. (2011). Global regression relations for conversion of surface wave and body wave magnitudes to moment magnitude. *Natural Hazards, 59*, 801–810, https://doi.org/10.1007/s11069-011-9796-6

Deniz, A., & Yucemen, M., S., (2010), Magnitude conversion problem for the Turkish earthquake data. *Natural Hazards, 55*(2) 333–352, https://doi.org/10.1007/s11069-010-9531-8

Dou, J.,Yunus, A.P., Bui, D.T., Merghadi, A., Sahana, M., Zhu, Z., Chen, C., Han, Z., & Pham, B.T. (2020). Improved landslide assessment using support vector machine with bagging, boosting, and stacking ensemble machine learning framework in a mountainous watershed, Japan. *Landslides*, *17* (3), 641–658. doi:10.1007/s10346-019-01286-5

Düntsch, I., & Gediga, G. (2019). Confusion Matrices and Rough Set Data Analysis. *Journal of Physics, Conference Series, 1229,* 012055. doi:10.1088/1742-6596/1229/1/012055

Eckert, N., Parent, E., Beˆlanger, L., & Garcia, S. (2007a). Hierarchical Bayesian modelling for spatial analysis of the number of avalanche occurrences at the scale of the township. *Cold Regions Science and Technology*, *50*(1–3), 97–112

Eckert, N., Parent, E., & Richard, D. (2007b). Revisiting statistical topographical methods for avalanche predetermination: Bayesian modelling for runout distance predictive distribution. *Cold Regions Science and Technology*, *49*(1), 88–107

Evans, I. (1972). General geomorphometry, derivatives of altitude, and descriptive statistics. In R.J. Chorley (Ed.), *Spatial analysis in Geomorphology (17-90)*. Methuen.

Feistl, T. (2015). Vegetation effects on avalanche dynamics. PhD Thesis, *Technical University at Munich,* DOI:10.13140/RG.2.2.11791.56484.

Fleiss, J.L. (1991). Statistical Methods for Rates and Proportions. *John Wiley and Sons*, Chichester

Ganju, A., Thakur, N.K., & Rana, V. (2002). Characteristics of Avalanche Accidents in Western Himalayan Region, India. *International Snow Science Workshop*, 2002: Penticton, B.C.

Ghinoi, A. & Chung, C.-J. (2005). STARTER: A statistical GIS-based model for the prediction of snow avalanche susceptibility using terrain features - Application to Alta Val Badia, Italian Dolomites. *Geomorphology, 66*. 305-325. 10.1016/j.geomorph.2004.09.018

Ghosh, S. (2011). Knowledge guided empirical prediction of landslide hazard: e-book. PhD thesis University of Twente; summaries in Dutch and English. *International Institute for*

Geo-Information Science and Earth Observation (ITC) Dissertation 190, *University of Twente*, ISBN: 978-90-6164-310-4

Ghosh, S. Carranza, E.J.M., van Westen, C.J., Jetten, V.G., & Bhattacharya, D.N. (2011). Selecting and weighting spatial predictors for empirical modeling of landslide susceptibility in the Darjeeling Himalayas (India). *Geomorphology, 131*, 35-56

Gill, J. C., & Malamud, B. D. (2016). Hazard interactions and interaction networks (cascades) within multi-hazard methodologies. *Earth System Dynamics, 7*, 659–679, https://doi.org/10.5194/esd-7-659-2016

Glade T. (2003). Landslide occurrence as a response to land use change: a review of evidence from New Zealand. *CATENA* 51:297–314.https:// doi. org/ 10. 1016/ S0341- 8162(02) 00170-4

Gupta, N., Kanungo, D. P., & Das, J. (2024). Multi-hazard susceptibility mapping of landslides and earthquakes in Bhagirathi Valley region of Uttarakhand Himalaya, India. *Journal of Spatial Science*, 1–26. https://doi.org/10.1080/14498596.2024.2409083

Gupta S, Kumar S, Wason HR, & Das R. (2012). A statistical analysis of completeness of earthquake data around Dehradun city and its implications for seismicity evaluation. *In: Proceedings of fifteen World Conference on Earthquake Engineering*, Lisbon, Portugal, Sept 24–28, 2012, paper no. 3539

Gutenberg, B., & Richter, C. F., (1954), Seismicity of the Earth and Associated Phenomena," *Princeton University Press*, Princeton

Guzzetti, F., Carrara, A., Cardinali, M., & Reichenbach, P. (1999). Landslide hazard evaluation: a review of current techniques and their application in a multi-scale study, Central Italy. *Geomorphology, 31*, 181-216

Guzzetti, F., Reichenbach, P., Cardinali, M., Galli, M., & Ardizzone, F., (2005), Probabilistic landslide hazard assessment at the basin scale. *Geomorphology,* 72, 272-299

Hagenlocher, M., Renaud, F.G., Haas, S., & Sebesvari, Z. (2018). Vulnerability and risk of deltaic social-ecological systems exposed to multiple hazards. *Science of The Total Environment, 631-632*, 71–80

Haque U, da Silva PF, & Devoli G., (2019), The human cost of global warming: deadly landslides and their triggers (1995–2014). Science of The Total Environment, 682:673–684. https:// doi. org/ 10. 1016/j. scito tenv. 2019. 03. 415

Hebertson, E. G., & Jenkins, M. J. (2003). Historic climate factors associated with major avalanche years on the Wasatch Plateau Utah. *Cold Regions Science and Technology*, 37(3), 315–332

IPCC. (2021). Summary for Policymakers. In V., P. Zhai, A. Pirani, S. L. Connors, C. Péan, S. Berger, N. Caud, Y. Chen, L. Goldfarb, M. I. Gomis, M. Huang, K. Leitzell, E. Lonnoy, J.B.R. Matthews, T. K. Maycock, T. Waterfield, O. Yelekçi, R. Yu and B. Zhou (Eds.), *Climate Change 2021: The Physical Science Basis. Contribution of Working Group I to the Sixth Assessment Report of the Intergovernmental Panel on Climate Change. Masson-Delmotte* (42). *Cambridge University Press*.

IS 1893 2016 Indian standard criteria for earthquake resistant design of structures. Part 1: General provisions and buildings; *Bureau of Indian Standards*, New Delhi.

Jasiewicz, J., & Stepinski, T.F. (2013). A pattern recognition approach to classification and mapping of landforms, *Geomorphology*, 182, 15 January 2013, 147-156

Jinxing, Z., Lixian, W., Baoyuan, X., Shimin, F., & Xilin, W. (2002). A study on the early—warning technique concerning debris flow disasters. *Journal Of Geographical Sciences, 12*, 363–370. https://doi.org/10.1007/BF02837558

Kala, C. P. (2014). Deluge, disaster and development in Uttarakhand Himalayan region of India-Challenges and lessons for disaster management. *International Journal of Disaster Risk Reduction, 8*, 143–152. https://doi.org/10.1016/j.ijdrr.2014.03.002

Kappes, M.S., Keiler, M., & von Elverfeldt, K., & Glade, T. (2012). Challenges of analyzing multi-hazard risk: a review. *Natural Hazards, 64*, 1925–1958. https://doi.org/10.1007/s11069-012-0294-2

Kaul M.K. (Ed) (1999). Inventory of the Himalayan Glaciers, *Special publication*, *34*, *Geological Survey of India*, 165

Kesarwani, K., Sharma, A, Ghosh, T, Kuniyal, J C, Tiwari, A, Mala, A, & Srivastava, V. (2021). Climate Change Impact on Himalayan Ecosystem: An Assessment of Rishiganga River Basin, Central Himalaya, India. *International Journal of Environmental Sciences*, *10* (4). 102-109. DOI: https://doi-ds.org/doilink/10.2020-51948721

Khan, I., Bahuguna, H. & Kainthola, A. (2024). Regional landslide susceptibility zonation utilizing bivariate statistical techniques in the northwestern Himalayas, Jammu and Kashmir, India. *Journal of Earth System Science, 133*, 157. https://doi.org/10.1007/s12040-024-02367-3

Khattri, K. N., Rogers, A. M., Perkins, D. M., & Algermissen, S. T. (1984). A seismic hazard map of India and adjacent areas. *Tectonophysics., 108*, 93–134. https://doi.org/10.1016/0040-1951(84)90156-2

Khattri KN. (1999). An evaluation of earthquakes hazard and risk in northern India. *Himalayan Geololgy,* 20:1–46

Kramer S L. (1996). Geotechnical earthquake engineering; *Prentice Hall*, Upper Saddle River

Kumar, P. Kumar, A. & Sinvhal, A., (2011). Assessment of seismic hazard in Uttarakhand Himalaya. *Disaster Prevention and Management, 20*, 531–542

Kumar, P., Shukla, B., Sharma, S., Kishtawal, C., & Pal, P.K. (2016). A high-resolution simulation of catastrophic rainfall over Uttarakhand, India. *Natural Hazards*, *80*. 10.1007/s11069-015-2013-2

Kumar, S., Srivastava, P. K., Snehmani, G., A., & Singh, M. K. (2016). Fuzzy-frequency ratio model for avalanche susceptibility mapping. *International Journal of Digital Earth*, *9*(12), 1168–1184

Kumar, S., Srivastava, P.K., & Snehmani. (2017). GIS-based MCDA-AHP modelling for avalanche susceptibility mapping of Nubra valley region, Indian Himalaya. *Geocarto International, 32*, 1254–1267

Kumar, S., Srivastava, P. K., Snehmani, & Bhatiya, S. (2019). Geospatial probabilistic modelling for release area mapping of snow avalanches. *Cold Regions Science and Technology, 165*, 102813. doi: 10.1016/j.coldregions.2019.102813

Kumar, V., Shukla, T., Mehta, M., Dobhal, D.P., Singh, B.M.P., & Nautiyal, S. (2020). Glacier changes and associated climate driver for the last three decades, Nanda Devi region, Central Himalaya, India, *Quaternary International*. doi: https://doi.org/10.1016/j.quaint.2020.06.017.

Kundu, V., & Patel, R. C. (2019). Susceptibility status of landslides in Yamuna valley, Uttarakhand, NW-Himalaya, India; *Himalayan Geology, 40(1*), 30–49.

Landrø, M., Hetland, A., Engeset, R. V., & Pfuhl, G. (2020). Avalanche decision-making frameworks: Factors and methods used by experts, *Cold Regions Science and Technology, 170*, 102897, https://doi.org/10.1016/j.coldregions.2019.102897.

Lee S., & Min K., (2001), Statistical analysis of landslide susceptibility in Yongin, Korea. *Environmental Geology, 40*, 1095-1113

Legendre, C.P., Tseng, T.L., Mittal, H., Hsu, C.H., Karakhanyan, A., & Huang, B.S. (2017). Complex wave propagation revealed by peak ground velocity maps in the Caucasus Area. *Seismological Research Letters*, *88*(3):812–821

Löbmann, M.T., Geitner, C., Wellstein, C., & Zerbe, S. (2020). The influence of herbaceous vegetation on slope stability – a review. *Earth-Science Reviews*, 209:103328. https:// doi. org/ 10. 1016/j. earsc irev.

MacMillan, R., Jones, R., & McNabb, D. (2004). Defining a hierarchy of spatial entities for environmental analysis and modeling using digital elevation models (DEMs). *Computers, Environment and Urban Systems, 28*, 175–200

Maggioni, M., & Gruber, U. (2003). The influence of topographic parameters on avalanche release dimension and frequency. *Cold Regions Science and Technology*, *37*(3), 407–419

Mahajan, A. K., Thakur, V. C., Sharma, M. L., & Chauhan, M. (2010). Probabilistic seismic hazard map of NW Himalaya and its adjoining area, India. *Natural Hazards*, *53*(3), 443–457. doi:10.1007/s11069-009-9439-3

Malakar, S. & Rai, A.K. (2023). Estimating seismic vulnerability in West Bengal by AHP-WSM and AHP-VIKOR, *Natural Hazards Research*, *3*(3), 464-473, ISSN 2666-5921, https://doi.org/10.1016/j.nhres.2023.06.001.

Malakar, M., Malakar, S., Hasan, M.S.U., Rai, A.K., & Kannaujiya, V.K. (2024). Seismic risk assessment using integrated MCDM method in West Bengal, India, *Evolving Earth*, *2*, , 100036, ISSN 2950-1172. https://doi.org/10.1016/j.eve.2024.100036.

Masi, E. B., Segoni, S., & Tofani, V. (2021). Root reinforcement in slope stability models: A review. *Geosciences, 11*(5), 212. https://doi.org/10.3390/geosciences11050212

Müller, F., Caflisch, T., & Müller, G. (1977). Instructions for the compilation and assemblage of data for a world glacier inventory: Zürich, *Swiss Federal Institute of Technology, Temporary Technical Secretariat for World Glacier Inventory, International Commission on Snow and Ice*, 28

Müller, F., Caflisch, T., & Müller, G. (1978). Instructions for the compilation and assemblage of data for a world glacier inventory — Supplement; identification/glacier number: Zürich, *Swiss Federal Institute of Technology, Temporary Technical Secretariat for World Glacier Inventory*, 7 ., plus app

Nagarajan, R., Venkataraman, G., & Snehmani. (2014). Rule based classification of potential snow avalanche areas. *Natural Resources and Conservation*, *2*(2), 11–24

Nath, S.K., Shukla, K. & Vyas, M. (2008). Seismic hazard scenario and attenuation model of the Garhwal Himalaya using near-field synthesis from weak motion seismometry. *Journal of Earth System Science, 117 (Suppl 2)*, 649–670 (2008). https://doi.org/10.1007/s12040-008-0062-6

Nath, S. K., & Thingbaijam, K. K. S. (2012). Probabilistic seismic hazard assessment of India. *Seismological Research Letters, 83*(1), 135–149. https://doi.org/10.1785/gssrl.83.1.135

NDMA. (2010). Development of probabilistic seismic hazard map of India; Technical report by *National Disaster Management Authority*, Government of India, New Delhi

Olaya, V.. (2009). Basic land-surface parameters. *In: Hengl, T., Reuter, H. (Eds.), Geomorphometry, Concepts, Software, Application. Elsevier*, pp. 141–169 (Ch. 6)

Owen, L.A., Benn, D.I., Derbyshire, E., Evans, D.J.A., Mitchell, W.A., & Richardson, S. (1996). The Quaternary glacial history of the Lahul Himalaya, northern India. *Journal of Quaternary Science, 11*(1), 25-42.

Ozay, B., & Orhan, O. (2023). Flood susceptibility mapping by best–worst and logistic regression methods in Mersin, Turkey. *Environmental Science and Pollution Research 30* (15), 45151–45170. https://doi.org/10.1007/s11356-023-25423-9.

Palemón-Arcos, L., Gómez-Arredondo, C. M., Damas-López, D. A., Chávez-Hernández, G., Gutiérrez-Can, Y., Hernández-Hernández, M. A., Bojórquez, E., & Barrera-Lao, F. (2020). Subsoil seismic characterization through Vs30 for future structural assessment of buildings (Ciudad del Carmen, Mexico), *Natural Hazards and Earth System Sciences*, Discuss. [preprint] https://doi.org/10.5194/nhess-2020-194, in review, 2020.

Pancholi, V., Bhatt, N., Singh, P., & Chopra, S. (2022). Multi-criteria approach using GIS for macro-level seismic hazard assessment of Kachchh Rift Basin, Gujarat, western India – First step towards earthquake disaster mitigation. *Journal of Earth System Science, 131*(3). https://doi.org/10.1007/s12040-021-01744-6

Pandey, P., Chauhan, P., Bhatt, C.M., Thakur, K.P., Kannaujia, S., Dhote, R.P., Roy, A., Kumar, S., Chopra, S., Bhardwaj, A., & Aggrawal, S.P. (2021). Cause and Process Mechanism of Rockslide Triggered Flood Event in Rishiganga and Dhauliganga River Valleys, Chamoli, Uttarakhand, India Using Satellite Remote Sensing and in situ Observations. *Journal of the Indian Society of Remote Sensing, 49*, 1011– 1024

Parra, E., Mohr, C.H., & Korup, O. (2021). Predicting Patagonian landslides: roles of forest cover and wind speed. *Geophysical Research Letters, 48*,1–10. https:// doi. org/ 10. 1029/ 2021G L0952 24

Petley, D. (2012). Global patterns of loss of life from landslides. *Geology, 40*, 927–930. https:// doi. org/ 10. 1130/ G33217.1

Pike, R. (1988). The geometric signature: quantifying landslide-terrain types from digital elevation models. *Mathematical Geology,* 20, 491–511

Pourghasemi, H.R., Gayen, A., Panahi, M., Rezaie, F., & Blaschke, T. (2019). Multi-hazard probability assessment and mapping in Iran. *Science of The Total Environment, 692*, 556–571

Pourghasemi, H.R., Kariminejad, N., Amiri, M., Edalat,M., Zarafshar,M., Blaschke, T., & Cerda, A. (2020). Assessing and mapping multi-hazard risk susceptibility using a machine learning technique. *Scientific Reports, 10*, 3203

Prashad, R., Srivastva, P. K., & Snehmani, Ganguly, A., Kumar, S., & Ganju, A. (2017). Snow Avalanche Susceptibility Mapping using Remote Sensing and GIS in Nubra-Shyok Basin, Himalaya, India. *Indian Journal of Science and Technology*, *10*(31), 1–12

Ram, P., Gupta, V., Devi, M., & Vishwakarma, N.(2020). Landslide susceptibility mapping using bivariate statistical method for the hilly township of Mussoorie and its surrounding

areas, Uttarakhand Himalaya. *Journal of Earth System Science, 129*, 167. https://doi.org/10.1007/s12040-020-01428-7

Rafique, A., Dasti, M. Y. S., Ullah, B., Awwad, F. A., Ismail, E. A. A., & Saqib, Z. A. (2023). Snow avalanche hazard mapping using a GIS-based AHP approach: A case of glaciers in Northern Pakistan from 2012 to 2022. *Remote Sensing, 15*(22), 5375. https://doi.org/10.3390/rs15225375

Rehman, A., Song, J., Haq, F., Mahmood, S., Ahamad, M. I., Basharat, M., Sajid, M., & Mehmood, M. S. (2022). Multi-hazard susceptibility assessment using the analytical hierarchy process and frequency ratio techniques in the Northwest Himalayas, Pakistan. *Remote Sensing, 14*(3), 554. https://doi.org/10.3390/rs14030554

Rout, M. M., Das, J., & Das, R. (2015). Probabilistic seismic hazard assessment of NW and central Himalayas and the adjoining region. *Journal of Earth System Science ,124*, 577–586

Rout, M. M., Das, J., & Das, R. (2018). Probabilistic seismic hazard for Himalayan region using kernel estimation method (zone free method), *Natural Hazards, 93*, 967–985

Rusk, J., Maharjan, A., Tiwari, P., Chen, T.H.K., Shneiderman, S., Turin, M., & Seto, K.C. (2022). Multi-hazard susceptibility and exposure assessment of the Hindu Kush Himalaya. *Science of The Total Environment*, *804*. doi:10.1016/j.scitotenv.2021.150039

Rusydi, M., Efendi, R., & Rahmawati, S. (2018). Earthquake Hazard Analysis Use Vs30 Data In Palu, *Journal of Physics, Conference. Series,* 979 012054

Satty, T.L. (1980). The analytic hierarchy process. New York, NY: *McGraw-Hill International Book Co*

Satty, T.L. (2000). The Fundamentals of decision making and priority theory with the analytic hierarchy process, Vol (VI). *Pittsburgh: RWS publications*; 478

Schweizer, J., Jamieson, J. B., & Schneebeli, M. (2003). Snow Avalanche Formation. *Reviews of Geophysics*, *41*(4), 1016

Sekhri, S., Kumar, P., Fürst, C., & Pandey, R. (2020). Mountain specific multi-hazard risk management framework (MSMRMF): Assessment and mitigation of multi-hazard and climate change risk in the Indian Himalayan Region, Ecol. *Indic., 118*, 106700, https://doi.org/10.1016/j.ecolind.2020.106700

Selçuk, L. (2013). An avalanche hazard model for Bitlis Province Turkey, using GIS based multicriteria decision analysis. *Turkish Journal of Earth Sciences*, *22*, 523–535

Sharma, S.S., & Ganju, A. (2000). Complexities of avalanche forecasting in western Himalaya–An overview. *Cold Regions Science and Technology*, *31*, 95–102

Sharma, V., & Sarkar, R. (2023). Evaluation of seismic hazard of Uttarakhand State of India through deterministic approach. *Journal of Earth System Science, 132*, 176. https://doi.org/10.1007/s12040-023-02185-z.

Sharma, L., & Kumar Rana, N. (2024). Prioritization of Susceptibility Zones for Multi-Hazard in Jammu Division of the North-West Himalayas, India for Disaster Risk Reduction. *IDRiM Journal, 14*(2), 1–30. https://doi.org/10.5595/001c.121460

Sharma, L., Rana, N. S. S, & Dube, S.K. (2024). Assessing Multi-hazard risk for disaster risk reduction in Jammu Division in North-West Himalayas, India. *Environmental Science and Pollution Research, 2024 Dec,31*(59), 66702-66724. doi: 10.1007/s11356-024-35539-1. Epub 2024 Dec 6. PMID: 39641848.

Shugar, D. H., Jacquemart, M., Shean, D., Bhushan, S., Upadhyay, K., Sattar, A., Schwanghart, W., McBride, S. K., Van Wyk de Vries, M., Mergili, M., Emmer, A., Deschamps-Berger, C., McDonnell, M., Bhambri, R., Allen, S., Berthier, E., Carrivick, J. L., Clague, J. J., Dokukin, M., Dunning, S. A., … Westoby, M. J. (2021). A massive rock and ice avalanche caused the 2021 disaster at Chamoli, Indian Himalaya. *Science, 373*(6552), 300–306. https://doi.org/10.1126/science.abh4455

Singh, D., & Ganju, A. (2008). Expert system for prediction of avalanches, *Current Science*, *94*, 1076–1081

Singh, V., Thakur, P. K., Garg, V., & Aggarwal, S. P. (2018). Assessment of Snow Avalanche Susceptibility of Road Network - A Case Study of Alaknanda Basin. *The International Archives of the Photogrammetry, Remote Sensing and Spatial Information Sciences, XLII-5*, 461–468

Sinha, R., & Sarkar, R. (2020). Seismic Hazard Assessment of Dhanbad City, India, by deterministic approach. *Natural Hazards, 103*, 1857–1880. https://doi.org/10.1007/s11069-020-04059-9

Skilodimou, H.D., Bathrellos, G.D., & Koskeridou, E. (2018). Physical and anthropogenic factors related to landslide activity in the northern Peloponnese, Greece. *Land, 7*:1–18. https:// doi. org/ 10. 3390/ land7 030085

Skilodimou, H.D., Bathrellos, G.D., Chousianitis, K., Youssef, A.M., Pradhan, B. (2019). Multi-hazard assessment modeling via multi-criteria analysis and GIS: a case study. *Environmental Earth Sciences, 78*, 47 (2019). https://doi.org/10.1007/s12665-018-8003-4

Snehmani, S. M. K., Gupta, R.D., & Ganju, A. (2013). DTM generation and avalanche hazard mapping using large format digital photogrammetric data and geomatics technique. *Journal of Remote Sensing and GIS, 4*(2): 4–13. ISSN: 2230-7990

Snehmani, B. A., Pandit, A., & Ganju, A. (2014). Demarcation of potential avalanche sites using remote sensing and ground observations: A case study of Gangotri glacier. *Geocarto International*, *29*(5), 520–535. https://doi.org/10.1080/10106049.2013.807304

Soe, M., Ryutaro, T., Ishiyama, D., Takashima, I., & Charusiri, K. W. I. P. (2009). Remote sensing and GIS based approach for earthquake probability map: A case study of the northern Sagaing fault area, Myanmar. *Journal of Geological Society, Thailland, 1*, 29-46.

Statham, G.; Haegeli, P.; Greene, E.; Birkeland, K.; Israelson, C.; Tremper, B.; Stethem, C.; McMahon, B.; White, B.; & Kelly, J. (2018). A conceptual model of avalanche hazard. *Natural Hazards, , 90*, 663–691

Ullah, F., Saqib, S.E., Ahmad, M.M., & Fadlallah, M.A. (2020). Flood risk perception and its determinants among rural households in two communities in Khyber Pakhtunkhwa, Pakistan. *Natural Hazards, 104*, 225–247

Ullah K., Wang Y., Fang Z., Wang L., & Rahman M. (2022). *Geoscience Frontiers, 13*, 101425. doi:10.1016/j.gsf.2022.101425

UN. (2002). Johannesburg Plan of Implementation of the World Summit on Sustainable Development, Technical Report. *United Nations*

UN-ISDR. (2005). Hyogo framework for action 2005–1015: building the resilience of nations and communities to disasters. *In World Conference on Disaster Reduction. Kobe, Hyogo, Japan*

UNISDR. (2015). Sendai Framework for Disaster Risk Reduction 2015-2030. *United Nations Office for Disaster Risk Reduction* (UNISDR).

Van Westen, C.J., Van Asch, T.W., & Soeters, R. (2006). Landslide hazard and risk zonation—why is it still so difficult?. *Bulletin of Engineering geology and the Environment*, 65,167-84

Wald, D.J., Quitoriano, V., Heaton, T.H., Kanamori, H., Scrivner, C.W., & Worden, C.B. (1999). TriNet "ShakeMaps": rapid generation of peak ground motion and intensity maps for earthquakes in southern California. *Earthquake Spectra, 15*(3), 537–555

Wang, Y., Fang, Z., Hong, H., & Peng, L. (2020a). Flood susceptibility mapping using convolutional neural network frameworks. *Journal of Hydrology, 582*, 124482

Wells, D. L., & Coppersmith, K. J. (1994). New empirical relationships among magnitude, rupture length, rupture width, rupture area and surface displacement; *Bulletin of the Seismological Society of America, 84*(4), 974–1002, https://doi.org/10.1785/BSSA0840040974

Wiemer, S., & Wyss, M. (2000). Minimum magnitude of completeness in earthquake catalogs: Examples from Alaska, the Western United States, and Japan; *Bulletin of the Seismological Society of America, 90*(4), 859–869, https://doi.org/10. 1785/0119990114

Wu, Y.M., Liang, W.T., Mittal, H., Chao, W.A., Lin, C.H., Huang, B.S., & Lin, C.M. (2016). Performance of a low-cost earthquake early warning system (P-alert) during the 2016 ML 6.4 Meinong (Taiwan) Earthquake. *Seismological Research Letters, 87*(5),1050–1059. https ://doi. org/10.1785/02201 60058

Wu, Y.M., Mittal, H., Huang, T.C., Yang, B.M., Jan, J.C., & Chen, S.K. (2018). Performance of a low-cost earthquake early warning system (P-alert) and shake map production during the 2018 Mw 6.4 Hualien (Taiwan) Earthquake. *Seismological Research Letters*, *90*(1)

Wubalem, A., & Meten, M. (2020). Landslide susceptibility mapping using information value and logistic regression models in Goncha Siso Eneses area, northwestern Ethiopia: *SN Applied Sciences*, *2*(5), 1-9.

Xi, N. & Mei, G. (2023). Avalanche Susceptibility Mapping by Investigating Spatiotemporal Characteristics of Snow Cover Based on Remote Sensing Imagery along the Pemo Highway—A Critical Transportation Road in Tibet, China. *Water, , 15,* 2743. https:// doi.org/10.3390/w15152743

Yilmaz, A. (2007). Environmental Geology. *Cumhuriyet University, Faculty of Engineering Publications*, Sivas, Publication No: 107

Yousefi, S., Pourghasemi, H.R., Emami, S.N., Pouyan, S., Eskandari, S., & Tiefenbacher, J.P. (2020). A machine learning framework for multi-hazards modeling and mapping in a mountainous area. *Scientific Reports*, 10, 12144 (2020). https://doi.org/10.1038/s41598-020-69233-2

Yule, G.U. (1912). On the methods of measuring association between two attributes. *Journal of the Royal Statistical Society*, *75*: 579-642

Zhu, J., Zhang, Y., Zhang, J., Chen, Y., Liu, Y., & Liu, H. (2023). Multi-Criteria Seismic Risk Assessment Based on Combined Weight-TOPSIS Model and CF-Logistic Regression Model—A Case Study of Songyuan City, China. *Sustainability*, *15*(14), 11216. https://doi.org/10.3390/su151411216